TOPICAL REVIEW

Quasinormal modes: the characteristic `sound' of black holes and neutron stars

Class. Quantum Grav. **16** (1999) R159–R216. Printed in the UK PII: S0264-9381(99)02941-X

TOPICAL REVIEW

Quasinormal modes: the characteristic 'sound' of black holes and neutron stars

Hans-Peter Nollert
Astronomy and Astrophysics, University of Tübingen, Tübingen, Germany

Received 22 March 1999, in final form 18 October 1999

Abstract. Gravitational waves emitted by perturbed black holes or relativistic stars are dominated by 'quasinormal ringing', damped oscillations at single frequencies which are characteristic of the underlying system. These quasinormal modes have been studied for a long time, often with the intent of describing the time evolution of a perturbation in terms of these modes in a way very similar to a normal-mode analysis. In this review, we summarize how quasinormal modes are defined and computed. We will see why they have been regarded as closely analogous to normal modes, and discover why they are actually quite different. We also discuss how quasinormal modes can be used in the analysis of a gravitational wave signal, such as will hopefully be detected in the near future.

PACS numbers: 0470B, 9760J, 0425N, 0440D

1. Introduction

Do black holes have a characteristic 'sound'? That is, do they have a distinct mode, or set of modes, of harmonic oscillations representing the time evolution of some initial displacement from their equilibrium state? Performing numerical studies of perturbations of a Schwarzschild black hole, Vishveshwara [1] found that they do; indeed, during a certain time interval, the evolution of some initial perturbation is dominated by damped single-frequency oscillations. The frequency and damping of these oscillations depend only on the parameters of the black hole (i.e. its mass in the Schwarzschild case), they are independent of the particular initial perturbation that excited them.

We are not surprised to find that a star can oscillate at frequencies which are characteristic for the particular star. These oscillations are carried by the fluid making up the star. A black hole, however, does not possess any material which could sustain such oscillations. While the horizon of a black hole is sometimes regarded as a kind of membrane, it is not the main 'carrier' of these oscillations, either. We will see that these oscillations essentially involve the spacetime metric *outside* the horizon.

On second thought, this is not as surprising as it may seem at first. It simply illustrates the fact that in general relativity, the spacetime does not merely provide the stage where physical processes occur. Rather, it is a dynamical entity itself, just like the fluid of a star. Even for neutron stars, we will discover that there exists an additional family of oscillation modes which is rather independent of the fluid and mainly involves the spacetime created by the star at equilibrium.

There are, however, important differences between a normal-mode system and these characteristic oscillations. They are not truly stationary, since they are damped quite rapidly.

0264-9381/99/120159+58$30.00

Furthermore, they seem to appear only over a limited time interval, rather than extending from arbitrary early to arbitrary late times, as normal modes do. For these reasons, they were dubbed 'quasinormal modes' (QNM) [2].

While first noticed in the context of black hole perturbations, the concept of quasinormal modes applies to a much broader class of systems. In particular, linear bound systems which are subject to damping will show such characteristic damped oscillations. An example which comes to mind immediately are oscillations of stars if internal damping is taken into account. Here, the quasinormal modes are very close to true normal modes which are obtained by ignoring the damping. In relativistic astrophysics, neutron stars show damped oscillations even if internal viscosity is ignored: energy is carried away by gravitational radiation, resulting in a damping of the star's oscillation. Again, there are undamped Newtonian modes which are very close to the damped relativistic modes, they can be regarded as the non-relativistic limit. However, we will see that the story is not quite that simple for neutron stars: in addition to their 'Newtonian' modes, they possess a second family of modes which is purely relativistic and does not occur in a Newtonian model.

Other physical systems showing quasinormal ringing include a vibrating string coupled to a surrounding medium, transmitting energy to infinity through this medium. Another example is an infinite torsion fibre whose moment of inertia changes along its length. Even laser cavities can be described in terms of quasinormal modes. Formally, all these systems are described by a wave equation (or a system of wave equations) containing either an additional potential or a variable refractive index.

In a normal-mode analysis, one usually has an ordinary differential equation, or a system of such equations, and imposes boundary conditions to the effect that the perturbation (or whatever wavefunction one is studying) must vanish outside a finite region in space. An example of such a system is a finite string fixed at both ends, otherwise isolated from its surroundings. This system is described by a self-adjoint operator with a discrete spectrum and a complete set of normal modes. Unfortunately, perturbations of black holes or neutron stars are quite different: the system we have is the metric outside the horizon in the case of a black hole, or metric and matter quantities over all space for neutron stars. The perturbations will propagate throughout all space; we cannot demand that they should be zero outside a finite region. Instead, we want to make sure that no gravitational radiation unrelated to the initial perturbation disturbs the system at late times. Therefore, we will impose outgoing boundary conditions, meaning that nothing is supposed to come in from spatial infinity or to come out of the horizon of the black hole. In the case of a neutron star, regularity conditions at the centre and matching conditions at the surface replace the boundary condition at the horizon.

Consequently, the spectrum of the corresponding operator is purely continuous. This seems to contradict the fact that single-frequency oscillations are observed in the time evolution of perturbations of black holes and neutron stars. We will see how quasinormal modes with isolated, characteristic frequencies can still be defined, in a way closely related to scattering resonances. However, these quasinormal modes will generally not form a complete set, in the sense that the time evolution of any initial perturbation could be described as a superposition of such quasinormal modes. It also becomes rather difficult to determine the excitation of quasinormal modes by given initial data. Even the boundary conditions themselves are very difficult to handle numerically.

Currently, several large interferometric gravitational wave detectors are under construction. Most of the signals that these detectors will 'see' can only be extracted from the noise if an accurate template exists for the expected signal. Therefore, a major effort is being made to obtain such templates by numerical, fully nonlinear simulations for processes such as colliding black holes [3, 4], collapsing or colliding neutron stars [5], or other systems that

are expected to emit strong gravitational radiation. Interestingly, quasinormal modes are again seen to dominate the gravitational radiation wave forms at certain times [6, 7], even though they are a concept born from linearized perturbation calculations. We can therefore regard them as a robust intrinsic feature of relativistic objects, rather than an artefact of the linearized perturbation treatment. As an alternative and complementary approach to the enormous effort necessary for the fully relativistic calculation of colliding black holes, Price and Pullin [8] have developed a close limit approximation based on perturbation techniques which has been amazingly successful.

All of these calculations demonstrate that quasinormal modes will play a prominent role in gravitational radiation emitted by a variety of astrophysical scenarios, and may well be seen by the new gravitational wave detectors. Consequently, a given signal may be analysed in terms of quasinormal modes, attempting to extract parameters such as oscillatory frequency and damping. These parameters may then be used to infer information about the system that produced these oscillations [9].

If we want to talk about how strongly some physical process excites quasinormal modes, we need to have a quantitative measure for such an excitation. This proves surprisingly difficult. In fact, there are ambiguities which cannot be resolved, since they are a consequence of the mathematical properties of quasinormal modes. Nevertheless, the possibility to use quasinormal modes to gain information, for example, about the mass and radius of a neutron star, or to distinguish between a black hole and a neutron star, is a very exciting astrophysical application of this mathematical concept.

This review focuses on the basic concept of quasinormal modes. We will restrict ourselves to the discussion of non-rotating black holes and neutron stars to avoid obscuring the picture with the added technical difficulties of treating rotating objects in general relativity. However, astrophysical objects will usually be rotating. In particular, there is currently a very interesting discussion about unstable modes of rotating neutron stars which do not exist for non-rotating stars. These may have a number of very interesting astrophysical consequences. In an appendix we will briefly summarize some of the work on rotating black holes and neutron stars and point the reader to relevant references.

2. The perturbation equation

In this section, we will demonstrate how the equations governing the perturbations of a Schwarzschild black hole can be derived, and how they can be reduced to a one-dimensional wave equation with a potential barrier. We will essentially follow the approach of Regge and Wheeler [10]; some errors in the original paper by Regge and Wheeler were later corrected by Edelstein and Vishveshwara [11].

The equilibrium state of a non-rotating (and uncharged) black hole is given by the well known Schwarzschild metric:

$$\mathrm{d}s^2 = -\left(1 - \frac{2M_\bullet}{r}\right)\mathrm{d}t^2 + \left(1 - \frac{2M_\bullet}{r}\right)^{-1}\mathrm{d}r^2 + r^2\,\mathrm{d}\theta^2 + r^2\sin^2\theta\,\mathrm{d}\varphi^2, \qquad (1)$$

where $M_\bullet$ is the mass of the black hole.

2.1. Linearized field equations

We regard the perturbed metric as a sum of the unperturbed background metric $\overset{\circ}{g}_{\mu\nu}$ and the actual perturbation $h_{\mu\nu}$:

$$\bar{g}_{\mu\nu} = \overset{\circ}{g}_{\mu\nu} + h_{\mu\nu}, \qquad (2)$$

where the perturbation is assumed to be small in some appropriate sense. At this point, the background metric can be any solution of the field equations; in particular, it does not need to be the Minkowski metric of flat spacetime. We will use the Schwarzschild metric later on, either for vacuum or for the interior of a spherically symmetric star.

Linearizing the Einstein equations in the perturbation h will yield equations for h in lowest order. Since we already know that the background metric satisfies the Einstein equations, we will now compute the Ricci tensor to first order in h. This task is simplified considerably if we only keep quantities up to linear order in h at each step. This is done by using the background metric to raise and lower indices on first-order quantities, such as

$$h^{\mu\nu} = \overset{\circ}{g}{}^{\mu\alpha}\,\overset{\circ}{g}{}^{\kappa\nu} h_{\alpha\kappa}. \tag{3}$$

Similarly, we will use the unperturbed Christoffel symbols in computing covariant derivatives of perturbation quantities.

From equation (3) it follows that

$$\bar{g}^{\mu\nu} = \overset{\circ}{g}{}^{\mu\nu} - h^{\mu\nu} + \mathcal{O}(h^2); \tag{4}$$

this can be verified directly by showing that $\bar{g}^{\mu\alpha}\bar{g}_{\alpha\nu} = \delta^{\mu}_{\nu} + \mathcal{O}(h^2)$.

The perturbed Christoffel symbols are given by

$$\bar{\Gamma}^{\kappa}{}_{\mu\nu} = \tfrac{1}{2}\bar{g}^{\kappa\alpha}(\bar{g}_{\alpha\nu,\mu} + \bar{g}_{\alpha\mu,\nu} - \bar{g}_{\mu\nu,\alpha}) = \overset{\circ}{\Gamma}{}^{\kappa}{}_{\mu\nu} + \delta\Gamma^{\kappa}{}_{\mu\nu} + \mathcal{O}(h^2), \tag{5}$$

where

$$\delta\Gamma^{\kappa}{}_{\mu\nu} = \tfrac{1}{2}\,\overset{\circ}{g}{}^{\kappa\alpha}(h_{\alpha\nu,\mu} + h_{\alpha\mu,\nu} - h_{\mu\nu,\alpha}) - \overset{\circ}{g}{}^{\kappa\alpha}\,\overset{\circ}{\Gamma}{}^{\beta}{}_{\mu\nu}\,h_{\alpha\beta}. \tag{6}$$

This can be rewritten as

$$\delta\Gamma^{\kappa}{}_{\mu\nu} = \tfrac{1}{2}\,\overset{\circ}{g}{}^{\kappa\alpha}(h_{\alpha\nu;\mu} + h_{\alpha\mu;\nu} - h_{\mu\nu;\alpha}). \tag{7}$$

The last equation reveals that the variation of the Christoffel symbols, $\delta\Gamma^{\kappa}{}_{\mu\nu}$, forms a tensor, even though the Christoffel symbols themselves do not.

Finally, we list the perturbation of the Ricci tensor:

$$\begin{aligned}\delta R_{\mu\nu} &= \delta\Gamma^{\alpha}{}_{\mu\alpha,\nu} - \delta\Gamma^{\alpha}{}_{\mu\nu,\alpha} + \delta\Gamma^{\beta}{}_{\mu\alpha}\overset{\circ}{\Gamma}{}^{\alpha}{}_{\nu\beta} + \overset{\circ}{\Gamma}{}^{\beta}{}_{\mu\alpha}\delta\Gamma^{\alpha}{}_{\nu\beta} - \delta\Gamma^{\beta}{}_{\mu\nu}\overset{\circ}{\Gamma}{}^{\alpha}{}_{\alpha\beta} - \overset{\circ}{\Gamma}{}^{\beta}{}_{\mu\nu}\delta\Gamma^{\alpha}{}_{\alpha\beta} \\ &= \delta\Gamma^{\alpha}{}_{\mu\alpha;\nu} - \delta\Gamma^{\alpha}{}_{\mu\nu;\alpha}.\end{aligned} \tag{8}$$

In vacuum, the perturbed field equations simply reduce to

$$\delta R_{\mu\nu} = 0. \tag{9}$$

These equations are explicitly linear in h, but they still form a system of ten coupled partial differential equations. Can we simplify them any further?

2.2. Separating the angular variables

Since the background is spherically symmetric, it is natural to assume that the equations governing the perturbations can be decoupled into separate equations describing the dependence of the angular variables θ and φ, on the one hand, and on the radial variable r and the time variable t, on the other hand.

The naive approach to that would be to expand each element of $h_{\mu\nu}$ separately in terms of spherical harmonic functions Y_{LM}. However, since the problem itself is not changed under rotations around the origin, the decomposition into spherical harmonics should also remain

unchanged under rotations. Writing out the transformation of h, it is obvious that this simple decomposition changes under rotation. Worse, it changes in a way that depends on the angular variables. As a result, the equations for the expansion coefficients still depend on the angular variables, defeating our purpose of decoupling them. This is not surprising, since this naive attempt does not recognize the symmetry of the original problem.

Instead, we have to decompose h into tensor functions which have the correct behaviour under rotations on the 2-sphere. Due to the symmetry of h, we need ten independent tensor functions $(Y^n_{LM})_{\mu\nu}$:

$$h_{\mu\nu} = \sum_{L=0}^{\infty} \sum_{M=-L}^{L} \sum_{n=1}^{10} C^n_{LM}(t,r)(Y^n_{LM})_{\mu\nu}(\theta,\varphi). \tag{10}$$

The task of finding these tensor functions is simplified considerably by noting that different parts of h transform differently under rotations. The parts marked 'S' in equation (11) transform like scalars under rotation, the parts marked 'V' like two-dimensional vectors and the part marked 'T' like a 2×2 tensor:

$$h = \begin{pmatrix} \boxed{\text{S}} & \boxed{\text{S}} & \boxed{\text{V}} \\ \boxed{\text{S}} & \boxed{\text{S}} & \boxed{\text{V}} \\ \boxed{\text{V}} & \boxed{\text{V}} & \boxed{\text{T}} \end{pmatrix}. \tag{11}$$

The scalar components of h can be represented directly by the scalar spherical harmonics, $Y_{LM}(\theta,\varphi)$. From the scalar function $S_{LM}(\theta,\varphi) = Y_{LM}(\theta,\varphi)$, vectors and tensors can be constructed as follows [10]:

$$\left(\overset{1}{V}_{LM}\right)_a = (S_{LM})_{;a} = \frac{\partial}{\partial x^a} Y_{LM}(\theta,\varphi) \tag{12}$$

$$\left(\overset{2}{V}_{LM}\right)_a = \epsilon_a{}^b\,(S_{LM})_{;b} = \gamma^{bc}\epsilon_{ac}\frac{\partial}{\partial x^b} Y_{LM}(\theta,\varphi) \tag{13}$$

$$\left(\overset{1}{T}_{LM}\right)_{ab} = (S_{LM})_{;ab} \tag{14}$$

$$\left(\overset{2}{T}_{LM}\right)_{ab} = S_{LM}\,\gamma_{ab} \tag{15}$$

$$\left(\overset{3}{T}_{LM}\right)_{ab} = \tfrac{1}{2}\left[\epsilon_a{}^c(S_{LM})_{;cb} + \epsilon_b{}^c(S_{LM})_{;ca}\right]. \tag{16}$$

The indices a, b, c run from 2 to 3; γ is the metric on the 2-sphere of radius 1, and ϵ is the totally antisymmetric tensor in two dimensions, i.e. $\epsilon = \sin\theta \left(\begin{smallmatrix} 0 & -1 \\ 1 & 0 \end{smallmatrix}\right)$; the covariant derivatives are to be taken on the 2-sphere.

Altogether, there is one scalar function which can be used in three places (taking into account the symmetry of h), two vectors which can be used in two places each and three tensors, for a total of ten independent contributions. The explicit tensor spherical harmonics constructed in this way have been given by Zerilli [12] and by Moncrief [13]. Note that only the tensors given by Zerilli form an orthonormal system under a suitable scalar product; the sets given in equations (12)–(16), which were also used by Regge and Wheeler [10] and Moncrief [13], are slightly different. The relationships between them can be found in Zerilli [12].

2.3. Parity

If we examine the individual contributions we have constructed in equations (12)–(16), we find that they have a distinct behaviour under space inversions. An inversion of space is achieved by letting $(\theta, \varphi) \to (\pi - \theta, \pi + \varphi)$. However, we can also formally set $(\theta', \varphi') = (\theta + \pi, \varphi)$. This immediately shows that the properties of Y_{LM} under inversion are independent of M. It can be verified directly from the definition of the Y_{LM} that they are multiplied by a factor of $(-1)^L$ under space inversions.

Usually, a (scalar) function which remains unchanged under space inversion is said to have even parity; if it simply changes sign, it has odd parity. However, in relativistic perturbation theory, functions acquiring a factor $(-1)^L$ under space inversions are often called even, and those with a factor $(-1)^{L+1}$ odd. To avoid confusion resulting from this discrepancy, Chandrasekhar refers to 'polar' $[(-1)^L]$ and 'axial' $[(-1)^{L+1}]$ perturbations instead [14] (chapter 4, section 24). He argues that changing the sign of φ—which achieves a space inversion followed by a rotation—shows that axial perturbations impart a differential rotation to the black hole, while polar perturbations do not. We will follow Chandrasekhar's terminology in this paper.

If we want to determine the parity of vectors and tensors, we cannot simply check how their components behave under space inversions, since this behaviour will depend on the chosen gauge. However, we can use the fact that taking the gradient of a function preserves parity, while multiplying with the totally antisymmetric tensor ϵ inverts it. The parity of the vector and tensor contributions is therefore as follows:

$$S_{LM} \quad \text{polar} \quad (-1)^L \tag{17}$$

$$\overset{1}{V}_{LM} \quad \text{polar} \quad (-1)^L \tag{18}$$

$$\overset{2}{V}_{LM} \quad \text{axial} \quad (-1)^{L+1} \tag{19}$$

$$\overset{1}{T}_{LM} \quad \text{polar} \quad (-1)^L \tag{20}$$

$$\overset{2}{T}_{LM} \quad \text{polar} \quad (-1)^L \tag{21}$$

$$\overset{3}{T}_{LM} \quad \text{axial} \quad (-1)^{L+1}. \tag{22}$$

Since the unperturbed metric is invariant against inversion, we expect that the perturbation equations will not mix polar and axial contributions. We can therefore separate a perturbation into polar and axial contributions and study them separately.

As an example, we list the general form of an axial perturbation with given L and M in a notation similar to that of Regge and Wheeler [10]:

$$h_{\mu\nu} = \begin{pmatrix} 0 & 0 & -h_0(t,r)\dfrac{1}{\sin\theta}\dfrac{\partial Y_{LM}}{\partial\varphi} & h_0(t,r)\sin\theta\dfrac{\partial Y_{LM}}{\partial\theta} \\ 0 & 0 & -h_1(t,r)\dfrac{1}{\sin\theta}\dfrac{\partial Y_{LM}}{\partial\varphi} & h_1(t,r)\sin\theta\dfrac{\partial Y_{LM}}{\partial\theta} \\ * & * & \frac{1}{2}h_2(t,r)\dfrac{1}{\sin\theta}X_{LM} & -\frac{1}{2}h_2(t,r)\sin\theta W_{LM} \\ * & * & * & -\frac{1}{2}h_2(t,r)\sin\theta X_{LM} \end{pmatrix}, \tag{23}$$

where the asterisks denote a component fixed by the symmetry of h, and

$$X_{LM}(\theta,\varphi) = 2\left(\frac{\partial}{\partial\theta}\frac{\partial}{\partial\varphi}Y_{LM} - \cot\theta\frac{\partial}{\partial\varphi}Y_{LM}\right) \tag{24}$$

$$W_{LM}(\theta,\varphi) = \left(\frac{\partial^2}{\partial\theta^2}Y_{LM} - \cot\theta\frac{\partial}{\partial\theta}Y_{LM} - \frac{1}{\sin^2\theta}\frac{\partial^2}{\partial\varphi^2}Y_{LM}\right). \tag{25}$$

Of course, there is one set of coefficient functions h_0, h_1 and h_2 for each L and M. For simplicity, we will not mark them as such explicitly.

2.4. The Regge–Wheeler gauge

The gauge of the background spacetime is essentially fixed, since we have decided to use the Schwarzschild metric in Schwarzschild coordinates. However, once we allow the background metric to be perturbed, we can change the gauge to first order in the perturbation, thereby affecting only the first-order metric perturbations, but not the background metric. We achieve this by using an infinitesimal gauge transformation

$$x'^{\mu} = x^{\mu} + \eta^{\mu} \tag{26}$$

where the gauge vector η is of first order in h. This results in

$$\begin{aligned} g'_{\mu\nu}(x') &= g_{\mu\nu}(x) + \eta_{\mu;\nu} + \eta_{\nu;\mu} - g_{\mu\nu,\alpha}\eta^{\alpha} \\ &= \overset{\circ}{g}_{\mu\nu}(x') + h_{\mu\nu} + \eta_{\mu;\nu} + \eta_{\nu;\mu} = \overset{\circ}{g}_{\mu\nu}(x') + h'_{\mu\nu}. \end{aligned} \tag{27}$$

Note that we always require the background metric to have the Schwarzschild form in whatever coordinates we are using. In other words, the functional form of the components $\overset{\circ}{g}_{\mu\nu}(x')$ after the coordinate transformation are required to be the same as $\overset{\circ}{g}_{\mu\nu}(x)$ before the transformation.

The signs in equation (27) correspond to the active form of the coordinate transformation, which is commonly used [15]; for the passive form, the sign of the gauge vector has to be inverted.

We want this gauge transformation to conserve both the decomposition into tensor spherical harmonics and the separation into polar and axial contributions. Therefore, we will construct one gauge vector in such a way that it is a polar vector under rotations, and one as an axial vector.

2.4.1. Axial gauge vector. We will discuss the axial gauge transformation as an example. The gauge vector has the form

$$\eta^{\mu} = \Lambda(t,r)\left[0, 0, \overset{2}{V}(\theta,\varphi)\right] = \Lambda(t,r)\left[0, 0, -\frac{1}{\sin\theta}\frac{\partial}{\partial\varphi}Y_{LM}, \sin\theta\frac{\partial}{\partial\theta}Y_{LM}\right]. \tag{28}$$

Explicitly computing the changes in the metric perturbation, using the unperturbed Christoffel symbols for the covariant derivatives in equation (27), we find that the new tensor $h'_{\mu\nu}$ has the correct general form (23) of an axial perturbation. The changes to the coefficients h_0, h_1 and h_2 are as follows:

$$\delta h_0 = \frac{\partial}{\partial t}\Lambda(t,r) \tag{29}$$

$$\delta h_1 = \frac{\partial}{\partial r}\Lambda(t,r) - 2\frac{\Lambda(t,r)}{r} \tag{30}$$

$$\delta h_2 = -2\Lambda(t,r). \tag{31}$$

We note that using a new coefficient k_1 instead of h_1, defined by

$$k_1 = h_1 + \frac{1}{2}\left(h_{2,r} - 2\frac{h_2}{r}\right), \tag{32}$$

results in

$$\delta k_1 = 0. \tag{33}$$

Therefore, k_1 is invariant under such an infinitesimal coordinate transformation. In general, there are many different ways to construct gauge-invariant functions from the coefficient functions h_0, h_1 and h_2. Moncrief [13] provides a decomposition of the metric perturbations into their gauge-invariant, gauge-dependent and constrained parts, using a variational principle to obtain the perturbation equations. It is the only invariant form that can be constructed from data related to a spatial hypersurface, i.e. from its intrinsic, three-dimensional metric and its extrinsic curvature (refer to section 5.2 for a brief description of these terms).

Regge and Wheeler have used the freedom of choosing a gauge to simplify the general form of the perturbations by eliminating the contribution with the highest derivatives in the angles (θ, φ). For axial perturbations, this means choosing the coefficient $h_2(t, r)$ to become zero. This is achieved by setting the function $\Lambda(t, r)$ as

$$\Lambda(t, r) = -\tfrac{1}{2}h_2(t, r). \tag{34}$$

We note that k_1 is equal to h_1 in the Regge–Wheeler gauge:

$$k_1(t, r) = (h_1)_{\mathrm{RW}}(t, r). \tag{35}$$

2.4.2. Polar gauge vector. The polar gauge vector has the following general form:

$$\begin{aligned}\eta^\mu &= \left[M_0(t, r)Y_{LM}(\theta, \varphi),\ M_1(t, r)Y_{LM}(\theta, \varphi),\ M_2(t, r)\overset{1}{V}(\theta, \varphi)\right] \\ &= \left[\ldots,\ \ldots,\ M_2(t, r)\frac{\partial}{\partial\theta}Y_{LM}(\theta, \varphi),\ M_2(t, r)\frac{1}{\sin^2\theta}\frac{\partial}{\partial\varphi}Y_{LM}(\theta, \varphi)\right].\end{aligned} \tag{36}$$

We now have three functions we can choose, allowing us to annul the coefficients of the $\overset{1}{V}$ and $\overset{1}{T}$ contributions (h_0, h_1 and G, in Regge and Wheeler's notation). Further details of the calculation are left to the reader as an exercise.

We note that given a perturbation in any gauge, we can immediately transform it into the Regge–Wheeler gauge point-by-point, without, say, having to solve any differential equations.

2.4.3. Regge–Wheeler gauge as conditions on h. We can also express the Regge–Wheeler gauge as conditions on the metric perturbation h:

$$\begin{aligned}&\frac{\partial}{\partial\theta}(\sin\theta\, h_{02}) = -\frac{\partial}{\partial\varphi}\left(\frac{1}{\sin\theta}\, h_{03}\right) \qquad && \frac{\partial}{\partial\theta}(\sin\theta\, h_{12}) = -\frac{\partial}{\partial\varphi}\left(\frac{1}{\sin\theta}\, h_{13}\right) \\ &h_{23} = 0 && h_{33} = \sin^2\theta\, h_{22}.\end{aligned} \tag{37}$$

This formulation applies to both axial and polar perturbation. Using equation (37), one can check whether a given metric perturbation is expressed in the Regge–Wheeler gauge without having to decompose it into tensor spherical harmonics first. On the other hand, it does not tell us how to determine the gauge vector needed to transform a given perturbation tensor into the Regge–Wheeler gauge.

2.5. Linearized equations for axial perturbations

Again, we will demonstrate the calculation for axial perturbations. The polar case follows the same general procedure, but it is more complicated technically because it involves a larger number of equations and unknown functions.

Inserting the axial perturbation tensor in its Regge–Wheeler form into the linearized field equations (9), we find that some equations are satisfied trivially, some are non-trivial only for $M \neq 0$ since the spherical harmonics $Y_{LM}(\theta, \varphi)$ appear only as derivatives with respect to φ, and some are non-trivial also for $M = 0$. Using the differential equation satisfied by the spherical harmonics,

$$\left(\sin^2\theta\frac{\partial^2}{\partial\theta^2} + \frac{\partial^2}{\partial\varphi^2} + \cos\theta\sin\theta\frac{\partial}{\partial\theta} + \sin^2\theta\, L(L+1)\right)Y_{LM}(\theta,\varphi) = 0, \qquad (38)$$

as well as its derivatives with respect to θ and φ, we can rewrite each component $\delta R_{\mu\nu}$ as a product of a radial function $R_i(t, r)$ and a non-vanishing angular function $A_i(\theta, \varphi)$. The results are summarized in table 1

Table 1.

Satisfied trivially:	$\delta R_{00} = \delta R_{01} = \delta R_{11} = 0$
Non-trivial condition for all values of M:	$\delta R_{23} = R_1(h_0, h_1, t, r)\, A_1(\theta, \varphi) = 0$
	$\delta R_{13} = R_2(h_0, h_1, t, r)\, A_2(\theta, \varphi) = 0$
	$\delta R_{03} = R_3(h_0, h_1, t, r)\, A_3(\theta, \varphi) = 0$
Non-trivial condition only for $M \neq 0$:	$\delta R_{22}, \delta R_{33}$: same condition as from δR_{23}
	δR_{12}: same condition as from δR_{13}
	δR_{02}: same condition as from δR_{03}

Specifically, these conditions are:

$$\delta R_{23}: \quad 0 = R_1(h_0, h_1, t, r) = \frac{1}{B(r)}\frac{\partial}{\partial t}h_0 - \frac{\partial}{\partial r}(B(r)h_1) \qquad (39)$$

$$\delta R_{13}: \quad 0 = R_2(h_0, h_1, t, r) \qquad (40)$$

$$= \frac{1}{B(r)}\left(\frac{\partial^2 h_1}{\partial t^2} - \frac{\partial^2 h_0}{\partial t\partial r} + \frac{2}{r}\frac{\partial h_0}{\partial t}\right) + \frac{1}{r^2}(L(L+1) - 2)h_1 \qquad (41)$$

$$\delta R_{03}: \quad 0 = R_3(h_0, h_1, t, r) \qquad (42)$$

$$= \frac{1}{2}B(r)\left(\frac{\partial^2 h_0}{\partial r^2} - \frac{\partial^2 h_1}{\partial t\partial r} - \frac{2}{r}\frac{\partial h_1}{\partial t}\right) + \frac{1}{r^2}\left(r\frac{\partial}{\partial r}B(r) - \frac{1}{2}L(L+1)\right)h_0, \qquad (43)$$

where $B(r) = (1 - 2M_\bullet/r)$.

It appears that we have three differential equations for only two unknown functions, $h_0(t, r)$ and $h_1(t, r)$. However, it turns out that this set of three equations contains some redundancy: any set of solutions of equations (39) and (41) will satisfy the time derivative of equation (43). There is a remaining ambiguity since h_0 appears only with its time derivative in equations (39) and (41), i.e. we can always add an arbitrary function of r to it. This additional function can then be determined using equation (43). In other words, equation (43) can essentially be derived from equations (39) and (41), the only additional information it provides is to fix an ambiguity left by equations (39) and (41).

2.6. The Regge–Wheeler equation

We may use equation (39) to eliminate h_0 from equation (41). Defining

$$Q_L(t,r) := \frac{1}{r}B(r)(h_1)_{\mathrm{RW}}(t,r) = \frac{1}{r}B(r)k_1(t,r), \tag{44}$$

we find that $Q(t,r)$ satisfies the following differential equation:

$$\frac{\partial^2 Q_L}{\partial t^2} - B(r)\frac{\partial}{\partial r}B(r)\frac{\partial}{\partial r}(rQ_L) + \frac{2}{r}B^2(r)\frac{\partial}{\partial r}(rQ_L) + \frac{1}{r}(L(L+1)-2)B(r)Q_L = 0. \tag{45}$$

We note that this equation depends on L, but not on M. This was to be expected due to the symmetry of the background, and due to the fact that it was sufficient to consider $M = 0$ to derive the radial equations (39)–(43).

We now switch to the tortoise coordinate

$$x = r + 2M_\bullet \ln\left(\frac{r}{2M_\bullet} - 1\right) \tag{46}$$

as the radial coordinate. This puts the horizon ($r = 2M_\bullet$) at $x = -\infty$, limiting the domain of the differential equation to the spacetime outside the horizon.

With this definition, equation (45) turns into

$$\frac{\partial^2}{\partial t^2}Q_L(t,x) - \frac{\partial^2}{\partial x^2}Q_L(t,x) + V_{\mathrm{RW}}(x)Q_L(t,x) = 0, \tag{47}$$

where

$$V_{\mathrm{RW}}(x) = \left(1 - \frac{2M_\bullet}{r(x)}\right)\left[\frac{L(L+1)}{r(x)^2} - \frac{6M_\bullet}{r(x)^3}\right] \tag{48}$$

is the so-called Regge–Wheeler potential. The equation describing axial perturbations now takes the form of a one-dimensional wave equation with an additional potential, called the Regge–Wheeler equation.

Note that just as for k_1, Q is invariant under first-order gauge transformations. Moreover, even though we have reduced the problem to this simple equation, we can still reconstruct the full axial perturbation (in the Regge–Wheeler gauge) from it. Besides h_1, we only need h_0, which can be obtained by integrating equation (39) and then using equation (43) to completely determine h_0.

2.7. Polar perturbations: the Zerilli equation

The analysis for polar perturbations proceeds along similar lines. It is, however, considerably more complicated due to the larger numbers of functions involved. Regge and Wheeler could not reduce the equations as far as those for axial perturbations, but Zerilli succeeded much later [12]. The result actually has the same form as the Regge–Wheeler equation, only the potential in the wave equation is different:

$$\frac{\partial^2}{\partial t^2}Z_L(t,x) - \frac{\partial^2}{\partial x^2}Z_L(t,x) + V_{\mathrm{Z}}(x)Z_L(t,x) = 0, \tag{49}$$

with

$$V_{\mathrm{Z}}(x) = \left(1 - \frac{2M_\bullet}{r}\right)\left[\frac{72M_\bullet^3}{r^5\lambda^2} - \frac{12M_\bullet}{r^3\lambda^2}(L-1)(L+2)\left(1 - \frac{3M_\bullet}{r}\right) + \frac{(L-1)\,L\,(L+2)(L+1)}{r^2\lambda}\right], \tag{50}$$

where $\lambda = L(L+1) - 2 + 6M_\bullet/r$ and $r = r(x)$.

The Regge–Wheeler and Zerilli potentials look rather different in their functional forms, but figure 1 shows that the actual values are quite close.

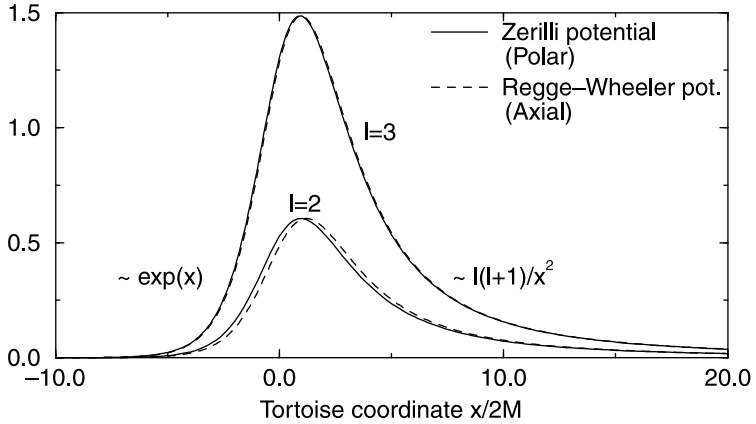

Figure 1. Regge–Wheeler and Zerilli potentials for $L = 2$ and 3.

It is truly amazing that after all this complicated analysis, we are left with just two one-dimensional wave equations which completely determine the behaviour of any perturbation of the black hole!

Even more astonishing is the fact that this holds true even if we consider a scalar or electromagnetic test field as the source of the perturbation [16]. Here, we study the dynamics of the field on the fixed background metric, discarding the influence that the energy–momentum tensor of this field has on the metric.

Again, the scalar or electromagnetic field is decomposed into appropriate spherical harmonics. The equation satisfied by the expansion coefficients, or suitable combinations thereof, is identical to the Regge–Wheeler equation, with only a simple parameter distinguishing between the three different cases:

$$V(x) = \left(1 - \frac{2M_\bullet}{r}\right)\left(\frac{L(L+1)}{r^2} + \sigma\frac{2M_\bullet}{r^3}\right) \tag{51}$$

$$\sigma = \begin{cases} +1 & \text{scalar test field} \\ 0 & \text{electromagnetic test field} \\ -3 & \text{axial gravitational perturbation.} \end{cases}$$

This can also be expressed by stating that $\sigma = 1 - \tau^2$, where $\tau \in \{0, 1, 2\}$ is the spin of the perturbing field.

2.8. Topics for further reading

- Using the Newman–Penrose formalism to derive the perturbation equations [17].
- Second-order perturbations [18].
- Perturbations of Reissner–Nordström black holes [19].
- The story of black hole perturbation (and other) research [20].

3. Time-independent perturbation equation and quasinormal modes

With the two wave equations (47) and (49) derived in the last section, we can determine the time evolution of any initial perturbation simply by integrating them numerically. However, we often want to study properties of the black hole itself, rather than the effect of a specific perturbation. One example is the question of whether black holes are stable. One way of doing this is by assuming a harmonic time dependence of the perturbations, studying the resulting time-independent perturbation equation. If it admits solutions whose amplitudes grow in time, then the black hole is unstable; otherwise, it is stable, at least under the assumptions made in this analysis.

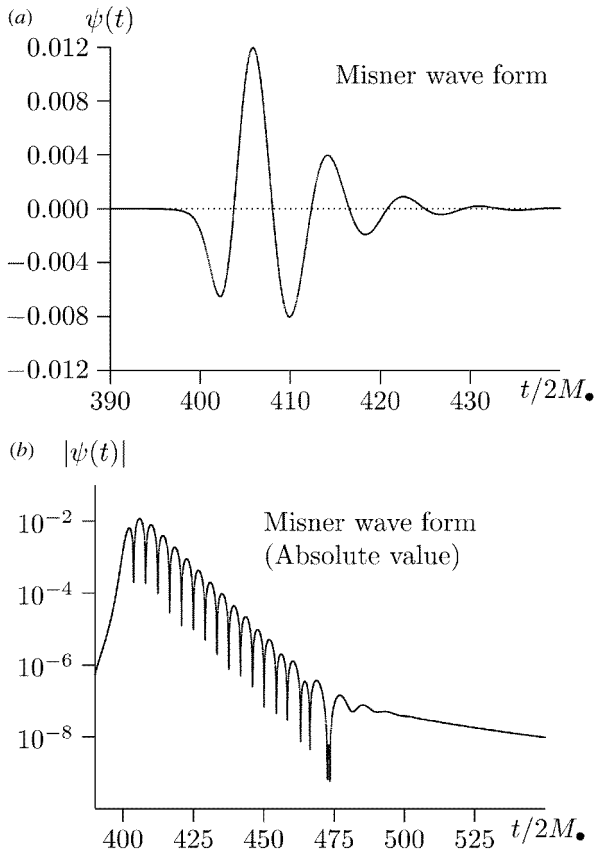

Figure 2. Time evolution of the Regge–Wheeler function for $L = 2$, on a linear (*a*) and a logarithmic (*b*) scale. The 'observer' is located at $r_{\rm obs} = 400 \times 2M_\bullet$.

Moreover, performing a numerical integration of the time-dependent wave equations leads to a rather surprising result. Figure 2 shows the result of such a calculation, both in a linear and a logarithmic representation. The initial perturbation arises from the close limit approximation for head-on black hole collisions [8], using a solution to the constraint equations found by Misner [21]. The most striking feature is the damped, single-frequency oscillation which dominates the wave form after an initial pulse has run its course, and before a power-law tail takes over at late time. Only one such frequency is clearly visible in the time evolution

shown in figure 2, but we will later see that a black hole actually possesses a multitude of such characteristic frequencies and corresponding quasinormal modes.

3.1. Fourier transformation

The damped single-frequency oscillation appears to be quite counter-intuitive: in contrast to a star, the black hole contains no material which could sustain such an oscillation, especially not outside its horizon. A straightforward tactic to investigate this mystery is to assume a harmonic time dependence for a perturbation and to study the conditions which allow such a solution to exist. In other words, we want to carry out a normal-mode analysis of black hole perturbations.

Following the standard procedure for such a normal-mode analysis, we will assume a solution of the perturbation equation with the harmonic time dependence $Q_\omega(t, x) = \mathrm{e}^{\mathrm{i}\omega t}\phi(x)$. Inserting this into the time-dependent wave equation (47) yields an ordinary differential equation in the radial coordinate:

$$\phi''(x) + \big(\omega^2 - V(x)\big)\phi(x) = 0, \tag{52}$$

where a prime denotes differentiation with respect to x. A general perturbation can then be represented as a continuous Fourier transform of such solutions. From now on, we will omit the subscripts L and M. Also, we will not explicitly distinguish between the Regge–Wheeler and the Zerilli equation, since this analysis applies to both cases.

Is it possible to reduce the continuous Fourier transform to a sum over individual frequencies, as in the case of a Sturm–Liouville problem such as the finite string? Both the Regge–Wheeler and the Zerilli potentials (cf figure 1) are positive everywhere, vanishing towards the horizon and towards spatial infinity. Therefore, they do not allow bound states: we cannot impose as boundary conditions that the solutions should vanish towards the boundaries (i.e. as $x \to \pm\infty$) [22].

This precludes a straightforward normal-mode analysis, as we have pointed out before. The spectrum of the associated operator will contain a continuous part. However, the prominence of single-frequency oscillations in the time evolution of perturbations suggests following an approach which mimics a normal-mode analysis. We will first describe a somewhat intuitive procedure and the problems that result from it, and then turn to a more systematic and mathematically rigorous definition of quasinormal modes.

As $|x|$ approaches infinity, the solutions of equation (52) will approach spherical plane waves, or more precisely, a combination of in-going and out-going spherical waves. This leads us to impose the conditions that towards the boundaries, the solutions should resemble purely out-going solutions [23], i.e.

$$\phi(\omega, x) \sim \mathrm{e}^{\mathrm{i}\omega x} \quad \text{as} \quad x \to -\infty \qquad \text{and} \qquad \phi(\omega, x) \sim \mathrm{e}^{-\mathrm{i}\omega \mathrm{x}} \quad \text{as} \quad \mathrm{x} \to \infty. \tag{53}$$

At the horizon, the term ‘out-going’ means ‘falling into the black hole’, thereby leaving the domain we are studying. Some authors, in fact, call the boundary condition at the horizon ‘in-going’, meaning the same condition as in equation (53). Keeping in mind that this analysis applies not only to black holes, but to all systems that can be described by a wave equation similar to (47) (or, as in the case of neutron stars, by some generalization thereof), we prefer the phrase ‘out-going at both boundaries’.

This choice of boundary conditions, even though imposed rather *ad hoc*, makes sense intuitively: we want to study the response of the metric outside the black hole to initial perturbations; we do not want gravitational radiation coming from infinity to continue

perturbing the black hole, and we assume that nothing can come through the horizon out of the black hole.

The discrete frequencies which allow solutions of equation (52) together with boundary conditions equation (53), are called quasinormal frequencies; the solutions constructed from them are the quasinormal modes. The 'normal' part in their names stems from the close analogy to normal modes in the way they are determined. The 'quasi' part expresses the fact that they are not quite the same; most notably, they are not really stationary in time due to their strong damping. Later we will see that there are several other important differences as well.

3.1.1. Stability of perturbations. Vishveshwara [24] has shown that equation (52) plus boundary conditions (53) cannot have any solutions where the frequency ω has a negative imaginary part. Wald [22] extended this argument into a rigorous proof that linear perturbations of the Schwarzschild metric must remain uniformly bounded for all time.

We will see that there are only discrete values of ω which allow solutions of equations (52) and (53); all of these have a non-vanishing, positive imaginary part. Again, this looks intuitively reasonable: a positive imaginary part of the frequency corresponds to a solution which vanishes exponentially with time. This is due to energy radiated away as gravitational radiation. On the other hand, a negative imaginary part would correspond to a bound state, which cannot exist due to the form of the potentials.

3.1.2. Problems. It almost looks like we have succeeded in finding a way to analyse perturbations of compact objects in terms of their characteristic frequencies and associated modes. Unfortunately, all is not well: the form of the boundary conditions (53) defining quasinormal modes means that they diverge exponentially towards infinity and towards the horizon. First of all, this is a major nuisance when trying to determine the frequencies and their modes numerically: the solution we are looking for is growing exponentially, and we need to determine whether it is contaminated by traces of the unwanted solution, which is *decreasing* exponentially as we approach the boundaries.

It turns out that this is, in fact, more than just a technical problem: in the way we have written them, each of the boundary conditions in equation (53) is not sufficient to single out just one solution of the differential equation (52); rather, they still admit a multitude of solutions. This aspect has been discussed in detail by Nollert and Schmidt [25, 26]. In short, equation (53) does not describe the desired solutions at any point in space; rather, it is an asymptotic expression specifying the limit behaviour as we approach infinity or the horizon. However, the unwanted solutions decay so fast as we approach the boundaries that they can always 'hide' behind the remainder term in the asymptotic expression. It is necessary to specify more precisely what we mean by a purely out-going solution, in order to turn it into a unique boundary condition.

We also encounter a problem if we try to determine how these quasinormal modes are excited by some initial perturbation. This is obviously an important step if we want to study the evolution of the perturbation in terms of quasinormal modes. In a normal-mode analysis, one usually represents the initial data as a sum over normal modes. This is possible since normal modes of a self-adjoint problem with a pure point spectrum—such as finite strings or membranes, or electromagnetic radiation in a finite cavity—form a complete set. Suppose, however, we have been given some initial perturbation of a black hole or neutron star as a function of space. This initial perturbation must be bounded in all of space. It is likely to be impossible to represent this initial data as a sum over quasinormal modes which diverge near the horizon of the black hole and towards spatial infinity.

One could also ask whether a quasinormal mode contains an infinite amount of energy, since it becomes infinite near the horizon and at spatial infinity. This problem is actually the easiest one to solve: a quasinormal mode could only have spread over all of space if it had existed for all of time. Due to the exponential decay with time, it would have had to be infinitely large at infinitely early time, which accounts for the infinite energy. This means that a single quasinormal mode is not a physical state of the system. Of course, it also means that we should not think in terms of a truly stationary solution, i.e. one that has existed forever and will continue to exist forever without changing. Rather, we will have to look explicitly at the time when the perturbation started, i.e. we will have to consider the initial data that excited the perturbation we are studying.

3.2. Laplace transform

The Fourier transform makes it very difficult for us to include this initial data in our study. In fact, when we started out, we did not want to include it, since we were interested in a general formalism that does not depend on the specific form of a perturbation and the initial data that caused it. However, it seems that we went a little too far in this attempt. So let us backtrack a little and include the initial data into the picture.

A technique that will allow us to do this, which is very similar to the Fourier transform, is the Laplace transform. If the initial data has compact support on the Schwarzschild part of the spacetime, then the solution of the perturbation equation will be bounded and allows a Laplace transform [27]. In general, this will remain true if the initial data are not compact, but sufficiently localized. The Laplace transform for a solution in the time domain is

$$\hat{f}(s,x) = \int_0^\infty \mathrm{e}^{-st}\, Q(t,x)\, \mathrm{d}t, \tag{54}$$

it is an analytic function of s for $\mathrm{Re}(s) > 0$.

The Laplace transform $\hat{f}(s,x)$ satisfies the differential equation

$$\hat{f}''(s,x) + \big(-s^2 - V(x)\big)\hat{f}(s,x) = \mathcal{I}(s,x), \tag{55}$$

where the source term $\mathcal{I}(s,x)$ is determined by the initial data:

$$\mathcal{I}(s,x) = -s\, Q\big|_{t=0} - \left.\frac{\partial Q}{\partial t}\right|_{t=0}. \tag{56}$$

Conversely, given a solution of equation (55), a solution of the time-dependent perturbation equation is obtained by

$$Q(t,x) = \frac{1}{2\pi \mathrm{i}} \int_{\varepsilon-\mathrm{i}\infty}^{\varepsilon+\mathrm{i}\infty} \mathrm{e}^{st}\, \hat{f}(s,x)\, \mathrm{d}s, \tag{57}$$

where the contour of integration runs parallel to, and just to the right of, the imaginary s-axis (see figure 4).

The solution of the inhomogeneous differential equation (55) is unique up to a solution of the homogeneous equation. Any two linearly independent solutions, say f_- and f_+, of the *homogeneous* differential equation

$$f''(s,x) + \big(-s^2 - V(x)\big) f(s,x) = 0 \tag{58}$$

define a particular Green's function $G(s,x,x')$ for the solution of the *inhomogeneous* equation, such that

$$\hat{f}(s,x) = \int_{-\infty}^{\infty} G(s,x,x')\, \mathcal{I}(s,x')\, \mathrm{d}x', \tag{59}$$

where

$$G(s, x, x') = \frac{1}{W(s)} f_-(s, x_<) f_+(s, x_>), \tag{60}$$

$x_< \equiv \min(x', x)$, $x_> \equiv \max(x', x)$ and $W(s)$ is the Wronskian of f_- and f_+: $W(s) = f_-(s, x) f'_+(s, x) - f'_-(s, x) f_+(s, x)$. If f_- and f_+ are solutions of a differential equation having the form of equation (58), the Wronskian does not depend on the variable x.

The homogeneous differential equation (58) has two linearly independent solutions, and each combination of them will produce a different Green's function and hence a different solution to the time-dependent perturbation equation (47). Which one is the correct one, i.e. the one that will result from the given initial data?

The boundedness of the solution in spacetime implies that its Laplace transform must be bounded in x as well. We will obtain a bounded solution from equation (59) if and only if f_- stays bounded as $x \to -\infty$ (i.e. at the horizon), and if f_+ stays bounded as $x \to +\infty$ (at spatial infinity), when s is in the right half of the complex plane.

If we examine equation (58) with standard techniques [28] (volume III.2, chapter V), it turns out that if $\mathrm{Re}(s) > 0$, a set of two linearly independent solutions, f_1 and f_2, exists such that f_1 stays bounded as $x \to -\infty$ while f_2 becomes unbounded. Therefore, all linear combinations of f_1 and f_2 with a non-vanishing contribution of f_2 will also be unbounded, and f_1 is essentially the only bounded solution. We must therefore choose f_- to be proportional to f_1. For $x \to +\infty$, the same occurs with another set of solutions. The choices for f_- and f_+ (and for the Green's function of equation (55)) are therefore uniquely determined by the boundedness of the original solution in spacetime. There is no need to impose *ad hoc* boundary conditions; the boundary conditions of the solutions we need to use are determined uniquely by the physics and mathematics of the problem.

We now know how to construct a solution of the perturbation equation, given specific initial data. Indeed, Leaver [29] and Sun and Price [30, 31] have shown how astrophysically realistic systems can be treated using the Laplace transformation. However, the quasinormal modes have somehow disappeared from our view. How can we identify them in the Laplace transform picture?

3.3. Topics for further reading

- Stability of non-rotating black holes [22, 27].

4. Quasinormal modes in the Laplace picture

A standard technique for identifying important contributions to the solution of a differential equation consists of closing the contour of integration in equation (57). This relates analyticity properties of the Laplace-transformed solution to the asymptotic behaviour of the time-dependent solution. If there are no essential singularities inside the contour, then the value of the integral along the closed contour (of which the original contour is a part) is equal to a sum over the residues inside the contour:

$$\oint \mathrm{e}^{st} \hat{f}(s, x)\, \mathrm{d}s = 2\pi \mathrm{i} \sum_q \mathrm{Res}\big(\mathrm{e}^{st} \hat{f}(s, x), s_q\big). \tag{61}$$

4.1. Quasinormal-mode expansion

Usually, one closes the contour with a half circle at infinity in either the right or left part of the complex plane. In fact, such a closure at $|s| = \infty$ should be regarded as the limit of a

sequence of closures at finite values of $|s|$. Let us assume for the moment that this sequence has a limit, and that the integral over the half circle at infinity vanishes in the limit. Furthermore, let there be no essential singularities inside the contour. Also, we assume that the solutions f_- and f_+ are analytic in s. These assumptions are satisfied in some simple cases, such as a square barrier potential, or an infinite torsion fibre with changing moment of inertia [32]. In general, one or more of them may be violated. In fact, we will see later that this is the case for the Regge–Wheeler and the Zerilli potentials. Nevertheless, it is instructive to use these simplifying assumptions at first, and come back later to the complications that arise when they do not hold.

With everything being analytic, the poles of the Green's function can only originate in zeros of the Wronskian $W(s)$. If these are simple roots, we can rewrite equation (61) as

$$\begin{aligned} Q(t,x) &= \frac{1}{2\pi\mathrm{i}}\int_{\varepsilon-\mathrm{i}\infty}^{\varepsilon+\mathrm{i}\infty}\mathrm{e}^{st}\int_{-\infty}^{\infty}G(s,x,x')\,\mathcal{I}(s,x')\,\mathrm{d}x'\,\mathrm{d}s \\ &= \frac{1}{2\pi\mathrm{i}}\oint\mathrm{e}^{st}\frac{1}{W(s)}\int_{-\infty}^{\infty}f_-(s,x_<)\,f_+(s,x_>)\,\mathcal{I}(s,x')\,\mathrm{d}x'\,\mathrm{d}s \\ &= \sum_q \mathrm{e}^{s_q t}\,\mathrm{Res}\left(\frac{1}{W(s)},s_q\right)\int_{-\infty}^{\infty}f_-(s_q,x_<)\,f_+(s_q,x_>)\,\mathcal{I}(s_q,x')\,\mathrm{d}x'. \end{aligned} \tag{62}$$

Specifically, if the initial data has compact support, and x is located to the right of this support, we have

$$Q(t,x) = \sum_q c_q u_q(t,x), \tag{63}$$

where

$$c_q = \frac{1}{\mathrm{d}W(s_q)/\mathrm{d}s}\int_{x_\mathrm{l}}^{x_\mathrm{r}}f_-(s_q,x')\,\mathcal{I}(s_q,x')\,\mathrm{d}x' \tag{64}$$

$$u_q(t,x) = \mathrm{e}^{s_q t}\,f_+(s_q,x), \tag{65}$$

with x_l and x_r denoting the left and right boundaries of the compact support of the initial data.

Such zeros do indeed exist in the left half of the complex s-plane. If $W(s=s_q)=0$, then the solutions $f_-(s_q,x)$ and $f_+(s_q,x)$ must be identical, up to a constant factor. Investigating equation (58) with standard techniques [28] (volume III.2, chapter V), we find that the solutions which are bounded at either end must behave like

$$\begin{aligned} f_-(s,x) &\sim \mathrm{e}^{sx}\left(1+\mathcal{O}\left(\frac{1}{x}\right)\right) \qquad \text{as} \quad x\to-\infty \\ f_+(s,x) &\sim \mathrm{e}^{-sx}\left(1+\mathcal{O}\left(\frac{1}{x}\right)\right) \qquad \text{as} \quad x\to+\infty \end{aligned} \tag{66}$$

in the right half-plane of s. Their analytic continuations into the left half-plane must therefore show the same behaviour, even though this will make them unbounded at the boundaries.

The formal replacement $s = \mathrm{i}\omega$ turns equation (58) into the Fourier-transformed differential equation (52). This replacement shows that f_- and f_+ satisfy the out-going quasinormal-mode boundary conditions of equation (53). Therefore, the vanishing of the Wronskian $W(s)$ for certain values of s (or ω) implies that the corresponding solution $f_- = f_+$ of the time-independent differential equation satisfies the conditions at *both* boundaries simultaneously. We may therefore identify such a solution with a quasinormal mode of a Schwarzschild black hole in the sense of the original, 'naive' definition based on equation (53).

While these zeros of the Wronskian are located in the left half of the complex s-plane, the boundary conditions for f_- and f_+ have been defined in the right half; their definition is then extended into the left half by virtue of analytical continuation in s of f_- and f_+.

We note that quasinormal frequencies of a real potential always come in complex conjugate pairs: if $f(s_q, x)$ is a quasinormal mode, then $f^*(s_q^*, x)$ satisfies the complex conjugate of the wave equation (58) as well as the boundary conditions (66). Consequently, the sums in equations (62) and (63) are real for any set of real initial data.

Equation (63) thus shows that any solution of the time-dependent wave equation can be represented completely by a sum over quasinormal-mode solutions. Therefore, under the assumptions we have made at the beginning of this section, these quasinormal modes form a complete set in the space of solutions.

This is the situation we are accustomed to with regard to systems of normal modes: they usually arise from a self-adjoint problem, forming a complete set of solutions which can be used to represent any solution of the problem. Specifically, at any time t, a solution can be represented by a sum over normal modes for all x in the domain of the differential operator. In particular, this also applies to $t = t_0$, i.e. we can expand the initial data in terms of the normal modes. However, this definition of completeness cannot be carried over directly to quasinormal-mode systems: the domain of the operator typically extends to infinity, where the quasinormal-mode solutions diverge. Solutions of the time-dependent problem, on the other hand, have to be bounded everywhere. As we have pointed out before, looking at the underlying physics, it would not make sense to talk about a solution spread out over all of space at a certain time. Such a perturbation would have to have existed since infinitely early time, having started out being infinitely large.

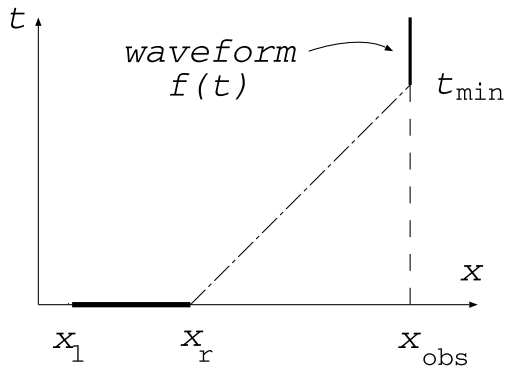

Figure 3. Propagation of initial data to the observation location $x_{\rm obs}$.

Instead, we focus on the time dependence of a solution at a fixed point in space (the location of an 'observer'). We will again consider initial Cauchy data with compact support, and for simplicity, we will locate the observer outside this area of support, and away from the maximum of the potential in the wave equation (figure 3). We take a complete quasinormal-mode system to be one which allows us to write the time dependence of any solution $Q(t, x)$, arising from such Cauchy data, at $x = x_{\rm obs}$ as a sum over quasinormal-mode solutions, as in equation (63).

4.2. Time-dependent expansion coefficients

Andersson [33] suggested that the early part of a wave form can be represented more accurately by a quasinormal-mode expansion if we allow the expansion coefficients to depend on time while the initial pulse is travelling past the observer, rather than requiring them to be constants as in equation (63).

This suggestion appears to be in direct contradiction with the principle that the time dependence of the wave form should be described by the time dependence of the modes we use in the expansion, while the coefficients should be constants which simply describe how much of each mode is 'contained' in the signal. If we allow time-dependent expansion coefficients, does the representation of the signal by quasinormal modes not become totally arbitrary, and therefore meaningless?

In fact, Andersson's proposal is well founded on the physics of the situation, and the scope of the quasinormal-mode representation that we have illustrated in figure 3. At a time $\bar{t}$, only the part of the initial data between $\bar{x}$ and x_{r} has reached the observer, the signal being seen cannot possibly be influenced by the second part of the initial data (between x_{l} and $\bar{x}$). Therefore, only the first part of the initial data should be used to determine the expansion coefficients for the signal at this point in time. As more of the initial data lies within the past lightcone of the observer, more of the initial data must be used to determine the expansion coefficient; consequently, the expansion coefficient will keep changing until all of the initial data has travelled past the observer:

$$c_q(t) = \frac{1}{\mathrm{d}W(s_q)/\mathrm{d}s} \int_{\bar{x}(t)}^{x_{\mathrm{r}}} f_-(s_q, x')\, \mathcal{I}(s_q, x')\, \mathrm{d}x'. \tag{67}$$

In contrast to a variable refractive index, the presence of the potential does not change the characteristics of the wave equation, and we simply have

$$\bar{x}(t) = \begin{cases} x_{\mathrm{r}} & (t \leqslant x_{\mathrm{obs}} - x_{\mathrm{r}}), \\ x_{\mathrm{obs}} - t & (x_{\mathrm{obs}} - x_{\mathrm{r}} < t < x_{\mathrm{obs}} - x_{\mathrm{l}}), \\ x_{\mathrm{l}} & (t \geqslant x_{\mathrm{obs}} - x_{\mathrm{l}}). \end{cases} \tag{68}$$

Therefore, the time dependence of the expansion coefficients is not arbitrary; rather, it is entirely fixed by the initial data and motivated in the physics of the configuration.

4.3. What is the 'right' way to construct a quasinormal-mode expansion?

In the previous two sections, we have encountered two rather different approaches to describing a signal, specifically to including its initial phase. The first approach uses a quasinormal-mode sum with constant expansion coefficients, focusing on the characteristic ring-down after the quasinormal modes have been excited by some initial data. We will call this the 'ring-down' picture. The other approach considers the build-up of the signal, and consequently of the expansion coefficients, as the initial data are propagated to the observer. We will call this the 'build-up' picture of quasinormal-mode expansion. The question naturally arises: which of these pictures is the 'correct' one?

In the 'build-up' picture, the propagation of information from the source to the observer is emphasized. The excitation of each quasinormal mode, at each point in time, is determined by that part of the initial data that had a chance to propagate to the observer at the given time. There is not much concern whether quasinormal ringing will be seen as dominating the resulting signal in a characteristic way at any time.

In the 'ring-down' picture, on the other hand, the analogy to normal modes is stressed. Quasinormal modes are seen as a property of the underlying system, rather than the initial data. It is regarded as significant that quasinormal modes show up as dominating the signal for some period of time in an obvious way. This requires that the expansion coefficients should be constants, they cannot be time dependent. The 'excitation' phase is completely dependent on the initial data, it does not really tell us anything about the underlying system and should therefore not be viewed in terms of quasinormal modes. It may be questioned whether a representation of the signal by quasinormal modes should even be attempted, in any way, during this initial phase.

The difference, then, is not one of right or wrong; rather, it is a question of the viewpoint, or the angle from which we want to approach the problem.

4.4. Incompleteness of quasinormal modes

Unfortunately, for perturbations of black holes and neutron stars, the situation is not as simple as we have pretended up to this point. Studies by Jensen and Candelas [34] and Ching *et al* [35] have shown that f_- is indeed analytic throughout the complex s-plane. However, f_+ has an essential singularity at $s = 0$. Furthermore, there is a branch cut extending from $s = 0$ to infinity. In addition, there are isolated singularities of f_+ along the negative imaginary s-axis. The difference in the behaviour of f_- and f_+ is related to the fact that the potential falls off exponentially in x as $x \to -\infty$, but much more slowly, as $1/x^2$, as $x \to +\infty$.

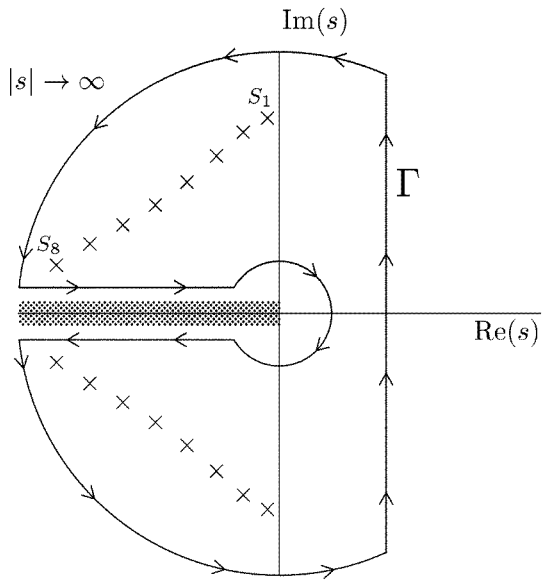

Figure 4. Path of integration Γ in the complex plane for the inverse Laplace transformation. $S_1 \ldots S_8$ are the first eight poles of the Green's function.

In order to keep the essential singularity at $s = 0$ from lying inside the closed contour, we choose the contour as shown in figure 4. The branch cut is usually positioned along the negative real s-axis; the half circle at $s \to \infty$ has to be split up into two quarter circles.

It turns out that the integration along the branch cut and around the essential singularity at $s = 0$ yields a non-vanishing contribution. The same is true for the quarter circles, even in the limit $s \to \infty$. We will discuss these contributions in more detail later. For now, we

note that their existence implies that the quasinormal modes of the Regge–Wheeler and the Zerilli potential do not form a complete set. This is actually true for most quasinormal-mode systems, except for a few such as those mentioned in section 4.1. In section 4.6, we will look at properties of the potential which allow, or preclude, a complete set of quasinormal modes.

4.5. Other contributions to the inverse Laplace transform for the Schwarzschild black hole

For a system with an incomplete set of quasinormal modes, we must modify equation (63) a bit:

$$Q(t, x) = \sum_q c_q u_q(t, x) + (\text{other contributions}). \tag{69}$$

The most important 'other contributions' are a power-law tail at late time, clearly evident in the time evolution of the Regge–Wheeler function in figure 2, and the prompt contribution, which is the initial perturbation propagated to the observer. They are related to specific parts of the integration path for the integral in equation (57). They have been studied extensively, for example, by Leaver [29] and Andersson [33]; we will just give a brief summary here.

4.5.1. Branch cut extending from the singularity at $s = 0$. The integration along the branch cut running from the singularity at $s = 0$ towards $|s| \to \infty$ along the negative real s-axis produces the power-law tail which dominates the signal at very late time. The tail is actually present throughout, but it is hidden by the quasinormal ringing. Only after the quasinormal modes, with their exponential decay, have become small enough, can the power-law tail take over.

Gundlach *et al* [36] have determined the exponents of the tails for various locations in the Schwarzschild spacetime. At spatial infinity, they find a leading decay as $t^{-(2L+3)}$. If the initial data are momentarily stationary on a null surface, this changes to $t^{-(2L+2)}$, or to $t^{-(2L+4)}$ if it is momentarily stationary on a Cauchy surface.

While the quasinormal-mode spectrum and the contribution of the quasinormal modes to the signal are related mostly to the form of the potential around its maximum, the power-law tail is determined by the long-range behaviour of the potential. Potentials falling off exponentially at large $|x|$ do not produce power-law tails [35]. Another, more specialized example is the truncated dipole potential which has an exact $2/x^2$ behaviour [37] for $x \geqslant x_0$.

4.5.2. Quarter-circles at $|s| \to \infty$. The integrals along the two quarter-circles at $|s| \to \infty$ generate the signal at early time, which is essentially the initial pulse being propagated through spacetime to the observer. In general, these contributions do not vanish. This means that the initial pulse usually cannot be described completely by the sum over the singularities of the Laplace transformed solution.

4.6. How properties of the potential affect completeness

Bachelot and Motet-Bachelot [38] have proven that a potential with compact support will not cause a power-law tail in the time evolution of Cauchy data. Beyer [39] has proven the same for the Pöschl–Teller potential. Ching *et al* [35] have argued that any potential falling off faster than exponentially towards infinity will not produce a power-law tail. In this case, completeness of the quasinormal modes depends only on the behaviour of the integral over the (now uninterrupted) half-circle at $|s| \to \infty$.

Using a WKB-type argument, Leung *et al* [40, 41] argue that the behaviour of this integral will be affected dramatically if there is a discontinuity in the potential or any of its derivatives. If that is the case, the Wronskian in equation (57) will eventually grow exponentially as $\mathrm{Re}(s) \to -\infty$, forcing the integral over the half-circle to vanish. The sum over the quasinormal modes will then completely describe the signal.

The potentials governing perturbations of black holes (and of the metric outside non-rotating neutron stars) do not fall off fast enough at spatial infinity, and they are smooth in all their derivatives. Therefore, the arguments above do not directly apply to them. Axial perturbations of neutron stars, though, can be described everywhere by a wave equation involving a potential, just as perturbations of black holes (cf section 5.2.1). This potential has a discontinuity at the surface of the star, either for the potential itself or for some derivative. The argument by Leung *et al* then implies that the quasinormal modes for axial perturbations of neutron stars should form a complete set, if the late-time power-law tail is subtracted from the wavefunction. Polar perturbations cannot be reduced to a 'wave equation plus potential' description, so the discontinuity argument is not directly applicable. It is possible, though, that the problem contains a discontinuity at the surface of the star which could have a similar effect to that of the discontinuity of the potential in the wave equation.

In the case of black holes, one can obviously introduce small modifications of the Regge–Wheeler or the Zerilli potential to ensure that they will satisfy the requirements for a complete set of quasinormal modes. We can first impose an exponential fall-off on the potential, starting at a very large radius, so that the potential as a whole is not changed considerably. If this manipulation is done correctly, it will not significantly disturb the spectrum of quasinormal modes [42]. Also, the time evolution of some Cauchy data should not be affected considerably by such a change. We mainly expect to see the tail eliminated, allowing the quasinormal ringing to continue indefinitely. However, this change may be regarded as insignificant with respect to the signal as a whole, since it occurs at a time when the amplitude of the signal has decreased by many orders of magnitude.

Second, we can introduce a small discontinuity into the potential. Nollert and Price [37] have studied such a modification extensively for the truncated dipole potential† as a model problem. It has not yet been applied to the actual problem of black hole perturbations.

If such a modification is kept small enough, we would expect the original quasinormal-mode spectrum to be almost unchanged, as well as the time evolution of the perturbation. How, then, can this set of quasinormal modes describe this time evolution completely, something that was not possible before the modification?

Phenomenologically, one can imagine the discontinuity as marking the boundary of a cavity. In fact, in the full-line case†, two such discontinuities are required, while one is sufficient in the half-line case. This cavity will have characteristic frequencies essentially determined by its width. These frequencies will show up in the spectrum in addition to the original quasinormal frequencies of the smooth potential, allowing the sum over all quasinormal modes to be complete.

† A truncated multipole potential is defined as

$$V(x) = \begin{cases} 0 & x \leqslant x_0 \\ L(L+1)/x^2 & x > x_0 \end{cases} \tag{70}$$

where $x_0 > 0$, L is a positive integer and $L = 1$ for the truncated dipole potential.

† The term full-line case refers to a problem being treated in, say, Cartesian coordinates, with the independent variable extending from $-\infty$ to $+\infty$. The half-line case corresponds to using polar coordinates, with the radial coordinate ranging from 0 to $+\infty$.

There is no strict mathematical proof for this conjecture, but it appears to be supported by various numerical calculations. The Regge–Wheeler and Zerilli potentials are both analytical everywhere, and we have seen that the quasinormal modes related to them are indeed not complete. This is already indicated by the simple fact that their frequencies are limited in the real parts, since this will probably make it impossible to represent the time evolution of initial data containing high-frequency components with such a set of modes. A similar argument applies to the truncated multipole potentials, which have only a finite number of quasinormal modes. However, if one introduces an additional discontinuity into, for example, the truncated dipole potential, it turns out that an additional set of frequencies appears in the spectrum [37], these new frequencies are unlimited in their real parts. Since the solutions for the truncated dipole potential are known analytically, it is possible to prove mathematically how the additional modes generate a complete set of solutions.

As an aside, we note that the one quasinormal mode of the truncated dipole potential actually describes the time evolution of any compact initial Cauchy data completely after the initial pulse has travelled past the observer (cf figure 3). Beyer [39] has proven a similar statement for the Pöschl–Teller potential which falls off exponentially as $x \to \pm\infty$. Moreover, if we adopt the 'build-up' picture with a time-dependent expansion coefficient as described in section 4.2, the quasinormal mode of the truncated dipole potential can be extended to describe all of the signal, including the initial pulse propagating past the observer. It is not known if this holds for the Pöschl–Teller potential as well. It does not work for the Regge–Wheeler potential, though [33].

For the Regge–Wheeler potential, Nollert [43] has taken the idea of introducing discontinuities to a natural extreme by replacing it with a step potential approximating the original one. Again, it turns out that the spectrum is now unlimited in the real parts of the frequencies, indicating that the set of quasinormal modes is now probably complete. Since a step potential has compact support, the Green's function has no branch cut, and there is no late-time power-law tail.

The spectrum of neutron stars shows such a branch without any modification of the original problem [44–46]. This occurs, in fact, for the physical problem as well as for a model problem studied earlier [47, 48]. Both for polar and axial perturbations, one can identify a branch of frequencies similar to the original black hole quasinormal frequencies as well as a branch being unlimited in the real parts [45, 49].

We should introduce one note of caution, however: in the case of the Regge–Wheeler potential being replaced by a step potential [43], it turns out that the quasinormal frequencies of the original potential, while still seen in the time evolution of a perturbation, are not recovered in the spectrum, even if the step size is made extremely small. A similar effect is seen if the truncated dipole potential is simply cut off at a finite distance, with the cut-off being moved to very large distances [37]. Leung *et al* have given an argument [50] as to why this should always apply if potentials are cut off at a finite distance. We therefore realize that it is possible to have a complete set of quasinormal modes, but its spectrum might be completely meaningless as far as an obvious connection with the time evolution of a perturbation is concerned.

4.7. Topics for further reading

- Model problem with complete set of QNM [32].
- Different concepts of completeness [41].
- Completeness of modes of Newtonian stars [51, 52].
- Power-law tail for perturbed dust collapse [53].
- Tails in nonlinear evolution [54].

5. Perturbation equations for neutron stars

Studying the comparatively simple example of perturbations of Schwarzschild black holes, we have gained an understanding of the basic concept of quasinormal modes and their significance in certain time evolution problems. Before we proceed to more technical issues, such as finding the values of quasinormal frequencies, quantifying excitations of quasinormal modes, or their use in the analysis of wave forms, we will first turn to perturbations of neutron stars and the role quasinormal modes play in this context.

5.1. Spherically symmetric equilibrium state

Due to the extra freedom associated with the material of the star, the determination of the equilibrium state of a neutron star is somewhat more involved than for a black hole. The following is only a brief summary; extensive discussions can be found in many standard textbooks on general relativity, e.g. Misner *et al* [55] and Weinberg [56].

We start by writing the general form of the metric (inside as well as outside the star) in the form

$$\mathrm{d}s^2 = (\mathrm{d}s^2)_0 = -\mathrm{e}^{\nu(r)}\,\mathrm{d}t^2 + \mathrm{e}^{\lambda(r)}\,\mathrm{d}r^2 + r^2\big(\mathrm{d}\theta^2 + \sin^2\theta\,\mathrm{d}\varphi^2\big). \tag{71}$$

Assuming that the material of the neutron star behaves like an ideal fluid, we have for the energy–momentum tensor

$$T_{\mu\nu} = pg_{\mu\nu} + (p+\rho)u_\mu u_\nu, \tag{72}$$

where $\rho(r)$ is the mass–energy density, $p(r)$ the pressure and u_μ the 4-velocity of the fluid.

Conservation of energy–momentum, i.e. the condition $T^{\mu}_{\nu;\mu} = 0$, yields

$$\frac{\mathrm{d}\nu}{\mathrm{d}r} = -2(\rho+p)^{-1}\frac{\mathrm{d}p}{\mathrm{d}r}. \tag{73}$$

Using the mass function $m(r)$, defined as

$$m(r) = \int_0^r 4\pi r'^2\rho\,\mathrm{d}r', \tag{74}$$

in connection with the field equations, we obtain

$$\mathrm{e}^{-\lambda} = 1 - \frac{2m}{r}. \tag{75}$$

Again using the field equations, as well as equation (73), we obtain the relativistic generalization for the condition of hydrostatic equilibrium:

$$\frac{\mathrm{d}p}{\mathrm{d}r} = -\frac{(\rho+p)(m+4\pi r^3 p)}{r(r-2m)}. \tag{76}$$

Equations (76) and (73), together with equation (74), are usually referred to as the Oppenheimer–Volkov (OV) or Tolman–Oppenheimer–Volkov (TOV) equations [55–57].

Using a barotropic equation of state for the star's material,

$$p = p(\rho), \tag{77}$$

completes the required equations for the determination of the unknown functions. Realistic equations of state are usually given numerically; either in the form of tables which must be

interpolated, or in the form of subroutines which compute the required values 'on the fly'. Polytropic equations of state are popular as analytic approximations, they have the form

$$p = K\rho^{1+1/n}, \tag{78}$$

where K is a constant, and n is called the polytropic index.

We can use the equation of state (77) to eliminate $p(r)$ from equation (76) and the differential form of equation (74), providing us with a system of two ordinary differential equations for the two unknown functions $\rho(r)$ and $m(r)$. One initial condition is given by $m(r = 0) = 0$. This leaves us with a choice for one additional parameter, for example, the central energy density $\rho(0)$. Spherically symmetric stars consisting of an ideal fluid (with given equation of state) therefore form a one-parameter family.

Using $m(r = 0) = 0$ and $\rho(0)$ as initial values, we integrate equations (76) and (74) outward from $r = 0$ until we reach a radius $r = R_{\text{star}}$ such that $p(r = R_{\text{star}}) = 0$, which defines the radius of the star. Once $\rho(r)$ and $m(r)$ are determined, we can use the equations above to find $p(r)$, $\lambda(r)$ and $\nu(r)$. Outside the star, we obtain, of course, the Schwarzschild metric with the mass parameter given by the total mass of the star:

$$M_{\text{star}} = \int_0^{R_{\text{star}}} 4\pi r^2 \rho \, \mathrm{d}r. \tag{79}$$

5.2. Perturbation of the star's equilibrium

We will again denote the perturbation of the metric by $h_{\mu\nu}(t, r, \theta, \varphi)$. In addition to the metric perturbation, we now have to deal with the perturbations of the energy density $\delta\rho$ and of the pressure δp. The Lagrangian change in the fluid velocity, which is just the velocity of the displacement of the fluid elements [57] (chapter 6.2), is called δu_μ.

Since $\delta\rho$ and δp are scalar quantities, the usual scalar spherical harmonics can be used for the separation of the angular variables θ and φ:

$$\delta\rho = E_\rho^{LM}(t, r) Y_{LM}(\vartheta, \varphi), \tag{80}$$

where a sum over L and M is implied. The pressure perturbation δp is determined from $\delta\rho$ via the equation of state:

$$\delta p = \frac{\mathrm{d}p}{\mathrm{d}\rho}\delta\rho = c_s^2 \delta\rho, \tag{81}$$

where c_s is the velocity of sound in the fluid.

Vector spherical harmonics are constructed in complete analogy with the tensor spherical harmonics as described in section 2.2. The representation of δu_μ becomes

$$\begin{aligned}
\delta u_0 &= U_0^{LM}(t, r) Y_{LM}(\vartheta, \varphi) = -\left(1 - \frac{2m}{r}\right) H_0^{LM}(t, r) Y_{LM}(\vartheta, \varphi) \\
\delta u_1 &= U_1^{LM}(t, r) Y_{LM}(\vartheta, \varphi) \\
\delta u_2 &= U_2^{LM}(t, r) \frac{\partial}{\partial\vartheta} Y_{LM}(\vartheta, \varphi) - U_3^{LM}(t, r) \frac{1}{\sin\vartheta} \frac{\partial}{\partial\varphi} Y_{LM}(\vartheta, \varphi) \\
\delta u_3 &= U_2^{LM}(t, r) \frac{\partial}{\partial\varphi} Y_{LM}(\vartheta, \varphi) + U_3^{LM}(t, r) \sin\vartheta \frac{\partial}{\partial\vartheta} Y_{LM}(\vartheta, \varphi).
\end{aligned} \tag{82}$$

The normalization of the 4-velocity has been used to determine u_0 in terms of H_0, which is related to the (tt) component of the metric perturbation.

Instead of writing out the complete expansion of the metric perturbation in terms of tensor spherical harmonics, we will just summarize which components of $h_{\mu\nu}$ are connected with which coefficient functions:

$$h_{\mu\nu} \rightarrow \begin{array}{c} \\ t \\ r \\ \vartheta, \varphi \end{array} \begin{array}{c} \begin{array}{ccc} t & r & \vartheta, \varphi \end{array} \\ \begin{pmatrix} H_0 & H_1 & h_0^{(\mathrm{p})}, h_0^{(\mathrm{a})} \\ * & H_2 & h_1^{(\mathrm{p})}, h_1^{(\mathrm{a})} \\ * & * & K, G, h_2 \end{pmatrix} \end{array}. \tag{83}$$

We are following the notation of Regge and Wheeler [10] here. Note that they use the symbols h_0 and h_1 both for coefficient functions of polar and axial perturbations; we distinguish them by superscripts (p) and (a).

The perturbation of the energy–momentum tensor can be expressed in terms of these quantities using equation (72) to first order in the perturbations.

We will use the field equations in their first-order form based on the ADM (3 + 1) decomposition of spacetime. An introduction to the ADM (3 + 1) formalism can be found in [55] (chapter 21.4ff) and [58]. In short, a four-dimensional spacetime is 'sliced' into three-dimensional spacelike slices which are stacked up along a timelike direction to fill up the whole spacetime. In this picture, the field equations take the form

$$\partial_t \gamma_{ij} = -2\alpha K_{ij} + \gamma_{ij,k}\beta^k + \gamma_{ki}\beta^k_{,j} + \gamma_{kj}\beta^k_{,i} \tag{84}$$

$$\begin{aligned} \partial_t K_{ij} = {} & \alpha\left[{}^3R_{ij} + K K_{ij} - 2K_{ik}K^k{}_j - 8\pi\left(T_{ij} - \tfrac{1}{2}T\gamma_{ij}\right)\right] \\ & -\alpha_{;j;i} + K_{ij,k}\beta^k + K_{ik}\beta^k_{,j} + K_{jk}\beta^k_{,i}. \end{aligned} \tag{85}$$

In addition to these dynamical equations, there are four equations which do not contain time derivatives. They have to be satisfied within each spatial slice, including the initial slice where we specify some initial perturbation. They are therefore called constraint equations:

$${}^3R - K_{ij}K^{ij} + K^2 = 16\pi T_{\mu\nu}n^\mu n^\nu = 16\pi\bar{\rho} \tag{86}$$

$$(K_{ij} - g_{ij}K)_{;i} = 8\pi T_{\nu j}n^\mu = 8\pi J_j, \tag{87}$$

where $\bar{\rho}$ denotes the total energy density and J_j the momentum density. Indices i, j run from 1 to 3, a semicolon (;) indicates covariant differentiation with respect to the geometry of the three-dimensional spatial slice, ${}^3R_{ij}$ and ${}^3R$ are the Ricci tensor and scalar curvature within this slice, $K = \mathrm{Tr}(K_{ij})$, etc. The three-dimensional metric γ_{ij} describes the geometry of each spatial slice, while the extrinsic curvature K_{ij} defines the way these slices are embedded in the four-dimensional spacetime. The lapse function α determines the 'distance' from one slice to the next along the time axis, while the shift vector β^k fixes the coordinates on each spatial slice. A specific choice of α and β^k corresponds to fixing a gauge. The normal vector n connects one slice to the next, it has the covariant components $(n_\mu) = (-\alpha, 0, 0, 0)$.

The relationship between $g_{\mu\nu}$, γ_{ij}, α and β^k is

$$g_{\mu\nu} = \begin{pmatrix} \beta_k\beta^k - \alpha^2 & \beta_j \\ \beta_i & \gamma_{ij} \end{pmatrix}, \tag{88}$$

i.e. γ_{ij} is just the spatial part of $g_{\mu\nu}$.

We therefore need to expand the (three-dimensional) extrinsic curvature in tensor spherical harmonics as well. Due to the static nature of the background metric, the perturbation of the

extrinsic curvature is identical to the total extrinsic curvature. We summarize the coefficient functions as follows:

$$\delta K_{ij} = K_{ij} \to \begin{array}{c} \\ r \\ \vartheta, \varphi \end{array} \begin{array}{c} \begin{array}{cc} r & \vartheta, \varphi \end{array} \\ \begin{pmatrix} K_1 & K_2, K_3 \\ * & K_4, K_5, K_6 \end{pmatrix} \end{array}. \tag{89}$$

Linearizing the field equations around the spherically symmetric background yields a system of first-order equations for the coefficients of these quantities. It can be written schematically as

$$\frac{\partial}{\partial t}\vec{Q}(t,r) = \underline{A}(r)\frac{\partial^2}{\partial r^2}\vec{P}(t,r) + \underline{B}(r)\frac{\partial}{\partial r}\vec{P}(t,r) + \underline{C}(r)\,\vec{P}(t,r). \tag{90}$$

Just as in the case of black holes, these equations depend on L, but not on M. Again, they separate into a set for polar perturbations and one for axial perturbations. The 'vectors' $\vec{Q}$ and $\vec{P}$ for these are

$$\begin{aligned} \vec{Q}^{\text{polar}} &= \left(H_2, h_1^{(\text{p})}, K, G, K_1, K_2, K_4, K_5, E_\rho, U_1, U_1\right) \\ \vec{P}^{\text{polar}} &= \left(H_0, H_1, H_2, h_0^{(\text{p})}, h_1^{(\text{p})}, K, G, K_1, K_2, K_4, K_5, E_\rho, U_1, U_2\right) \end{aligned} \tag{91}$$

$$\begin{aligned} \vec{Q}^{\text{axial}} &= \left(h_1^{(\text{a})}, h_2, K_3, K_6, U_3\right) \\ \vec{P}^{\text{axial}} &= \left(h_0^{(\text{a})}, h_1^{(\text{a})}, h_2, K_3, K_6, U_3\right). \end{aligned} \tag{92}$$

(Note that the symbol K in equation (91) denotes a coefficient function in the expansion of the metric perturbation H in terms of tensor spherical harmonics; it has nothing to do with the extrinsic curvature tensor K_{ij}.)

$\underline{A}$, $\underline{B}$ and $\underline{C}$ are given in terms of the functions $\rho(r)$, $p(r)$, $m(r)$, $\nu(r)$ and $\lambda(r)$ of the background equilibrium star (cf [59] for the explicit equations for a specific set of variables). Since the background star is usually computed numerically, the functions describing it are also given numerically.

In the first-order system, we only need the spatial components of the perturbation tensor h. The coefficient functions H_0, H_1, $h_0^{(\text{p})}$ and $h_0^{(\text{a})}$ relate to parts of h where at least one index is timelike. They nevertheless appear in equations (91) and (92) since they are connected with the lapse and the shift vector, which occur explicitly in equations (84). However, they are missing in the 'vector' $\vec{Q}$ on the left-hand side of the evolution equations. Therefore, we do not have any equations fixing their time derivatives, and we cannot evolve them in time. They will have to be determined by making a first-order gauge choice, and again, we will use the Regge–Wheeler gauge for this purpose.

As we have seen in section 2.4, the Regge–Wheeler gauge results in the coefficient functions $h_0^{(\text{p})}$, $h_1^{(\text{p})}$, K and h_2 becoming zero. In addition, some of equations (84) reduce to simple algebraic relations: H_0 is given in terms of H_2, H_1 in terms of K_2, $h_0^{(\text{a})}$ in terms of K_6 and K_4 vanishes together with $h_0^{(\text{p})}$. This not only fixes the coefficient functions H_0, H_1, $h_0^{(\text{p})}$ and $h_0^{(\text{a})}$, it also determines four additional functions and satisfies four of equations (84) identically. We are now left with a total of 12 equations for 12 unknowns. Eight of these describe polar perturbations, and the remaining four axial perturbations.

These sets of unknown functions and equations can be manipulated in a variety of ways in order to simplify them further, or to obtain systems of equations which are more suitable for numerical integration. Different combinations of unknowns and equations are used by different authors [59–63]. We will not present any of them explicitly; rather, we will give a short summary of the general procedures and results.

5.2.1. Axial perturbations. In the case of axial perturbations, the equation for U_3, the only matter coefficient involved, has a very simple solution

$$U_3(t, r) = f(r). \tag{93}$$

This solution represents stationary, differential rotations. Since we assume the star to consist of an ideal fluid, there are no restoring forces between adjacent fluid shells which could lead to oscillations or to braking of the rotation. Furthermore, this motion does not give rise to gravitational radiation. Therefore, metric perturbations are decoupled from matter perturbations in the axial case.

The equations for the matter perturbation coefficients can be reduced to a wave equation for a single coefficient. This equation depends on the background metric, but not on other perturbation quantities. The situation is therefore much the same as for black holes: the neutron star simply provides the background for the evolution of the metric perturbations, but, at least to first order, it is not influenced by them. There is no horizon, of course; the boundary condition at the horizon is replaced by a regularity condition at the origin ($r = 0$).

Axial perturbations of neutron stars have been studied by Chandrasekhar and Ferrari [64] and by Kokkotas [46].

5.2.2. Polar perturbations. Equations (90) and (92) represent eight partial differential equations which are of first order in t, but their right-hand sides still contain second derivatives with respect to r. Introducing further auxiliary functions results in a hyperbolic system of 12 partial differential equations which are of first order in space and time.

This system has six eigenvalues which are different from zero, they come in three pairs having equal absolute value and opposite sign. They represent three dynamical degrees of freedom, two of which are associated with gravitational radiation, and one with matter oscillations. They can be represented by three constrained wave equations. If one specifies initial data for these wave equations, the constraints must be solved explicitly; the wave equations themselves preserve the constraints during the time evolution. Alternatively, Moncrief [62] has eliminated the constraints from the equations; this leads to two unconstrained, coupled second-order wave equations.

The equations governing polar perturbations cannot be simplified further by analytical means. They must be integrated numerically, using conditions for regularity at the origin, for continuity at the star's surface and for out-going radiation at spatial infinity as boundary conditions.

5.3. Topics for further reading

- Perturbation equations and boundary conditions form a well posed Cauchy problem [65].
- Two unconstrained coupled wave equations for polar perturbations [60–62].
- Decoupling the hydrodynamical variables from the metric perturbations [63].
- Axial perturbations of neutron stars [64].
- Stability of stars against radial perturbations [55] (chapter 26).
- Stability of Newtonian and relativistic stars [57] (chapter 6, also section 17.2) and [66, 67].
- Stability of rotating and non-rotating stars [68, 69].

6. Computing quasinormal frequencies

After discussing the basic concept of quasinormal modes and their relevance to perturbations of relativistic objects, we will now turn to the task of finding the actual values of quasinormal

frequencies, that is, to computing the quasinormal-mode spectrum of black holes and neutron stars.

6.1. Quasinormal frequencies of black holes

We have seen that both polar and axial perturbations of black holes are governed by wave equations, but the potentials appearing in these wave equations are different. Chandrasekhar has shown that solutions of one equation can be transformed into solutions of the other [70]. Moreover, transmission and reflection amplitudes, as functions of frequency, are identical for the two. Therefore, the quasinormal frequencies of polar and axial perturbations have to be identical. In fact, such a relation applies to a much broader class of potentials [71]. Price and Anderson [72] have approached this question from a somewhat different angle, suggesting that such an equivalence relation is not as exotic an occurrence as one might expect at first. This equivalence makes it irrelevant whether the methods for computing quasinormal frequencies of black holes described in the following apply to polar or axial perturbations, or to both.

Even though the equations defining quasinormal frequencies of black holes look innocent enough, it turns out to be rather difficult to determine the actual values of these frequencies. It has not been possible to find analytical solutions of equation (47) or (52). Numerical calculations suffer mainly from the problem we have already mentioned in section 3.1.2: quasinormal modes are defined by the boundary conditions they satisfy at the horizon and at spatial infinity. Therefore, we need to examine the solutions of the time-independent wave equation (52) near these boundaries, where they diverge exponentially. Moreover, we have to make sure there is no contamination by the unwanted solution, which decreases exponentially. This presents a major stumbling block for computations which are limited to finite accuracy.

6.2. Analysing solutions of the time-dependent wave equation

One way to circumvent this problem is to look directly at a wave form that results from integrating the time-dependent wave equation, such as the one shown in figure 2. If one uses compact initial data, it is always possible to extend the computational domain far enough so that the signal never reaches the boundary during the time one is evolving the perturbation. Therefore, the out-going boundary condition is enforced implicitly, without ever having to impose it explicitly.

Davis *et al* [73] found that the signal generated by a particle falling into a Schwarzschild black hole shows ringing dominated by a frequency with $\mathrm{Re}(\omega M) = 2/\sqrt{27} \approx 0.385$. Cunningham *et al* [53] have studied a perturbed Oppenheimer–Snyder collapse; they extracted the first two $L = 2$ frequencies from the emitted gravitational radiation. Using artificial initial perturbations, Bachelot and Motet-Bachelot [42] could determine three quasinormal frequencies for $L = 2$ and four for $L = 3, 4$.

The major drawback of this approach is that only frequencies showing prominently in the time-evolved wave form can be identified. To some extent, this can be induced by selecting appropriate initial data. However, strongly damped modes are covered up too quickly by other modes or other contributions to the wave form, such as the power-law tail. Therefore, only a few frequencies for each value of L can be obtained. It remains unknown how many there are, whether their number is finite or infinite, and whether the frequencies themselves occupy a bounded or unbounded region in the complex plane.

6.3. Analysing the time-independent wave equation

6.3.1. The straightforward approach. Chandrasekhar and Detweiler [74] used asymptotic series approximations for each of the appropriate solutions near the boundaries. These were used as initial values for a numerical integration of the phase function (the logarithmic derivative of the Zerilli function) towards a common point near the maximum of the potential. If the Wronskian of these solutions vanishes for a particular value of ω, then the solutions are identical up to a constant factor. Therefore, this solutions satisfies both boundary conditions simultaneously, and ω is a quasinormal frequency.

Once again, in its original form, this approach allows only the determination of frequencies with moderate imaginary parts, i.e. the imaginary parts cannot be much larger than the real parts of the frequencies. They found two frequencies for $L = 2$ and three for $L = 3, 4$, but some of these turn out to be rather inaccurate and may be numerical artefacts.

6.3.2. Variations. Nollert and Schmidt [26] extended this approach by using much more elaborate representations for the behaviour of the solutions near the boundaries and for the Wronskian between them. The solution satisfying the boundary condition at the horizon is represented by a power series which actually converges far from the black hole where there is no problem with exponential divergence. This solution is then followed towards spatial infinity. Even though there is no such convergent power series for the solution with the correct behaviour at infinity, they could construct a convergent series representation for the Wronskian of these two solutions, which can be evaluated numerically. Again, if this Wronskian vanishes for some value of ω, then ω is a quasinormal frequency. They determined 12 frequencies for $L = 2$, with the largest imaginary part being about 35 times as large as the corresponding real part.

Fröman *et al* [75] suggested allowing the radial variable r to become complex, using an angle in the complex r-plane such that the product ωr is real. Integrating the wave equation along this line, instead of along the real r-axis, both the out-going and in-going solutions are purely oscillatory; they neither diverge nor die away as $|r|$ becomes large. This avoids the numerical problems and makes identification of the appropriate solutions easier.

Using a systematic formalism based on this idea, called the 'phase–amplitude' method, Andersson [76] calculated 11 quasinormal frequencies of a Schwarzschild black hole for $L = 2, 3$.

6.4. Analytical approximations

Mashhoon *et al* avoided the problem of having to deal with the boundary conditions numerically by approximating the Regge–Wheeler potential in the wave equation (52) with other potentials which allowed them to solve the problem analytically, as well as identifying the out-going solutions exactly. They used a harmonic oscillator potential [77], a Pöschl–Teller potential [78] and an Eckart potential [79].

The idea is that these potentials contain free parameters which can be adjusted to obtain a good fit to the Regge–Wheeler potential near its maximum. This results in a good approximation of the fundamental frequencies, and a reasonable idea of a few higher frequencies. However, the more highly damped modes also have longer wavelengths, and are more sensitive to changes in the potential far away from its maximum. Therefore, the frequencies with large imaginary parts proved elusive once more.

6.5. WKB-type techniques

Schutz and Will [80] modified the standard WKB technique to allow the determination of quasinormal modes. The key point is that two WKB solutions are matched across both turning points simultaneously, with the function $\omega^2 - V(x)$ being approximated by a polynomial between the turning points. They obtain a formula for ω_n, where n is an index counting frequencies for a given L. They find good agreement with other numerical calculations for $n = 0$, but not for larger values of n.

Carrying this approach to third WKB order and using a better approximation for $\omega^2 - V(x)$, Iyer and Will [81, 82] obtained an improved formula for ω_n. They provide numerical values up to $n = 6$ which agree well with other numerical calculations. The accuracy decreases with increasing n as the turning points move away from the peak of the potential, rendering the approximation for $\omega^2 - V(x)$ less accurate.

Guinn *et al* [83] expressed the transmission amplitude in terms of a contour integral of WKB functions around the turning points. In principle, this should work well for large values of n. They show numerical results up to $n = 58$. While the imaginary parts of the frequencies are reproduced by their technique, the real parts disagree significantly with other numerical calculations [26, 76, 84, 85].

Fröman *et al* [75] employed a phase-integral method involving an arbitrary-order phase-integral approximation generated from some base function and the use of the F-matrix method for the connection problem, again working in the complex r-plane. They obtained accurate quasinormal frequencies for n up to 5, but the accuracy deteriorates with increasing n.

Andersson and Linnæus [85] improved the phase-integral method including a third transition point as well as a second-order pole at the horizon, and employing uniform approximations by parabolic Weber functions and Coulomb wavefunctions. This allowed them to determine frequencies with very large imaginary parts. They provide results up to $n = 50$, large enough to develop an idea of the asymptotic behaviour of the frequencies for arbitrarily large n.

6.6. Continued fractions

Leaver took a completely different route: he recognized that the time-independent wave equation (52) has the same form as the Schrödinger equation for the H_2^+ ion. The major difference is that for the H_2^+ ion, the boundary conditions define a self-adjoint problem; one looks for bound states which remain finite at the boundaries. It turns out that the eigenvalues of this problem have to satisfy a continued fraction relation; the functions appearing in the continued fraction are given by the recurrence relation which determine the coefficients in a certain series representation of a specific solution of the differential equation. Leaver [84] adapted this formalism to the computation of quasinormal modes for black holes.

This analogy between bound states of H_2^+ and quasinormal modes of a black hole is not as straightforward as it appears from a formal point of view: bound states vanish at the boundaries, while quasinormal modes diverge exponentially. Therefore, the problem that lies at the root of the numerical difficulties does not exist for bound states to begin with. Nevertheless, the method turns out to work very well numerically.

While the convergence of the continued fraction still depends on the imaginary part of the frequency, it is not nearly as sensitive as the techniques employed before. Leaver calculated frequencies up to $n = 60$ [84], but the method can be extended beyond that. Table 2 and figure 5 show results obtained with this method; they indicate that the set of quasinormal frequencies is countably infinite, and that the frequencies are not bounded to a finite part of the complex

Table 2. The first four quasinormal frequencies of a black hole for $L = 2, 3, 4$.

n	$2M_\bullet\omega$ $(L = 2)$	$2M_\bullet\omega$ $(L = 3)$	$2M_\bullet\omega$ $(L = 4)$
0	0.747 343 + 0.177 925i	1.198 887 + 0.185 406i	1.618 36 + 0.188 32i
1	0.693 422 + 0.547 830i	1.165 288 + 0.562 596i	1.593 26 + 0.568 86i
2	0.602 107 + 0.956 554i	1.103 370 + 0.958 186i	1.545 42 + 0.959 82i
3	0.503 010 + 1.410 296i	1.023 924 + 1.380 674i	1.479 68 + 1.367 84i

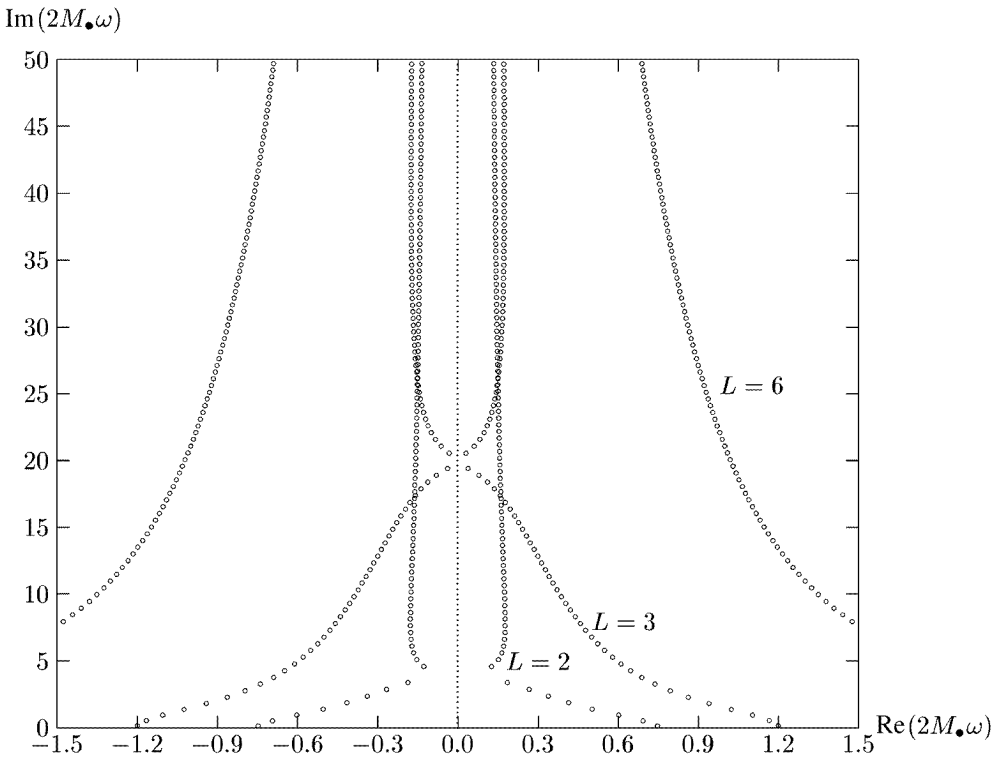

Figure 5. Quasinormal frequencies of a black hole for different values of L. For $L = 6$, the lowest frequencies lie beyond the range of the figure; the frequencies 'cross' the imaginary axis at $\mathrm{Im}(\omega) = 280$.

plane. While their real parts appear to be bounded (in fact, the fundamental frequency is the one with the largest real part), the imaginary parts can grow arbitrarily large.

6.7. Limiting cases for the frequencies

6.7.1. Fundamental mode and small imaginary parts. Mashhoon [77] derived an approximate formula for the fundamental quasinormal frequency ($n = 0$) and frequencies with small imaginary parts (small n):

$$(2M_\bullet\omega_n)^2 \approx 4V(x_{\max}) - 4\mathrm{i}\left(n + \tfrac{1}{2}\right)\left(-2\frac{\mathrm{d}^2V}{\mathrm{d}x^2}(x_{\max})\right)^{1/2}, \tag{94}$$

where the peak of the potential barrier is located at $x_{\max}$.

Schutz and Will [80] later arrived at the same formula using a WKB approach of scattering at the peak of the potential barrier.

6.7.2. Large imaginary parts: the large-n limit. Leaver's results provide a qualitative idea about the asymptotic behaviour of quasinormal frequencies for large n, but details are still unclear: will the frequency approach the imaginary axis, or a finite real part? Does their asymptotic behaviour depend on L? Nollert [86] introduced a further variation to the continued fraction technique which solved the convergence problem for very large imaginary parts of the frequencies. This allowed him to compute 100 000 frequencies without reaching a limit of the method. It turned out that the real parts of the frequency approach a finite limit, while the imaginary parts grow with an essentially constant increment. The leading order is independent of L:

$$2M_\bullet\omega_n \approx 0.087\,4247 + \tfrac{1}{2}\left(n + \tfrac{1}{2}\right)\mathrm{i} + \mathcal{O}\left(n^{-1/2}\right). \tag{95}$$

This result was confirmed by Andersson [87] using the improved phase-integral method [85]. Liu [88] derived an analytic expression for the imaginary part which confirms the leading order of the results of Nollert and Andersson and agrees well in the following orders. He could not obtain the limit value of the real part, however. It remained unclear, whether this finite limit for the real parts of the frequencies has any physical significance. Recently, Hod [89] has used Bohr's correspondence principle to link the oscillation frequency of the asymptotic quasinormal modes to the area spacing of a quantum black hole.

Bachelot and Motet-Bachelot [42] (see also [38]) have proven rigorously that there is indeed a countably infinite number of quasinormal modes of a Schwarzschild black hole. However, their proof does not give any indication about the behaviour of the mode frequencies for large n.

6.7.3. The large-L limit. For a given upper limit on the imaginary part, $0 \leqslant \mathrm{Im}(\omega) \leqslant \Gamma_0$), corresponding to an upper limit on n ($n \leqslant N_{\max}$), the limit behaviour for large values of L can be determined analytically [78]. It is given by

$$2M_\bullet\omega_n \approx 2L + 1 + \mathrm{i}(2n + 1). \tag{96}$$

Owing to the limitation in $\mathrm{Im}(\omega)$ (or n), this formula cannot be compared directly to the large-n limit (95).

6.8. Calculating the residues

Calculating the residues in equation (64) for the Green's function appears to be a straightforward task. In practice, it is even more difficult than obtaining the quasinormal frequencies themselves, since the derivative of the Wronskian with respect to the frequency must be evaluated. Leaver [29] has given numerical values for $L = 2, 3, 4$ and n up to 7. Andersson [90] found values which agree with Leaver's generally within better than 10% as far as the absolute values are concerned, but they frequently have the opposite sign. This discrepancy has not yet been resolved conclusively, but Andersson's results appear to be confirmed by an alternative numerical calculation.

6.9. Topics for further reading

- Relationship between quasinormal modes and bound states of the inverted potential [91].
- Matrix WKB method [92].

- Review of the phase-integral method [93].
- Why the Bohr–Sommerfeld formula fails for large n [94].
- Generalized Bohr–Sommerfeld formula [95].
- Algebraically special frequencies [96, 97].
- Highly damped frequencies [86–88].
- Quasinormal frequencies of perturbed potentials [98].

6.10. Quasinormal modes of neutron stars

Using again the harmonic time dependence $e^{i\omega t}$ for all perturbation quantities, we can Laplace transform the two coupled wave equations mentioned in section 5.2.2 and obtain a fourth-order system of differential equations. This system can then be analysed for quasinormal-mode solutions in a way analogous to the black hole case, as discussed in section 3.2. Historically, Thorne and Campolattaro [99] first derived a fifth-order system of ordinary differential equations. Detweiler and Lindblom [100] later showed that this can be reduced to a system of four first-order equations.

Unlike the black hole case, we do not have a horizon now, and the domain of integration therefore ranges from $r = 0$ to $r \to \infty$. The following conditions are imposed on an oscillation mode of the star:

- The solution has to be regular at the centre ($r = 0$).
- The Lagrangian change of pressure must vanish at the surface of the star.
- The solution corresponds to purely out-going radiation at $r \to \infty$.

A typical procedure is to start with a representation of the solutions which are regular at $r = 0$ ([101], appendix) as an initial condition for the perturbation equations inside the star, integrating them outwards from $r = 0$. At the surface of the star, the Zerilli function is determined from the perturbation quantities, and then the Zerilli equation is integrated towards $r \to \infty$. The boundary condition at $r \to \infty$ can then be checked with the same methods used for computing quasinormal modes of black holes.

6.11. Fluid modes

We expect neutron stars, unlike black holes, to have a set of modes associated with the fluid of the star. These modes also exist in the non-relativistic limit of the star. If we assume a non-relativistic star to consist of an ideal fluid and ignore internal dissipation, these oscillations will continue undamped forever, since there is no gravitational radiation to carry away energy. A relativistic star loses energy through gravitational radiation, but due to the weak coupling of gravity to matter, this loss should be slow compared to the period of oscillation. We can therefore expect a set of modes with oscillation periods close to their Newtonian counterparts, and a damping rate which is small compared to the inverse oscillation period. Chandrasekhar and Ferrari [102] have shown how the Newtonian modes can be recovered in a relativistic treatment by letting the star become less and less relativistic.

There are actually a variety of different families of fluid modes. For a non-rotating star consisting of an ideal fluid with a barotropic equation of state, the following are relevant:

- The fundamental mode, or f-mode, consists of non-radial surface waves. There is only one f-mode, it is nearly independent of the details of the stellar structure. For a typical neutron star, it has a frequency of a few kHz, the damping time for a relativistic f-mode is a few tenth of a second.

- Pressure modes, or p-modes, are radial or non-radial oscillations where pressure supplies the restoring force. There are infinitely many of them. The lowest p-mode typically has a frequency of around 5 kHz and a damping time of a few seconds. Their frequencies increase monotonically with the order of the mode. Damping times also tend to increase with the order of the mode, but not monotonically.

Numerous studies have dealt with computing these fluid modes (for example, see [99, 100] and references therein).

6.12. 'Wave' modes

It turns out that relativistic neutron stars have another family of modes which does not have a Newtonian counterpart. These modes were first identified by Kokkotas and Schutz [44]. They called them w-modes (gravitational wave modes) since they are mostly related to perturbations of the metric of the spacetime, rather than oscillations of the star's fluid. These metric perturbations contain less energy and couple more directly to gravitational radiation. Therefore, their energy is radiated away much faster, and they are much more strongly damped than the fluid modes. A second family of w-modes was later identified by Leins *et al* [45] and confirmed by Andersson *et al* [103]. Figure 6 shows the frequencies of both the fluid modes and the w-modes of a typical relativistic neutron star, determined by Andersson *et al* [103]. Note that the w-mode frequencies are unbounded in their real parts. This could allow the w-modes to represent high-frequency contributions in the gravitational wave signal.

While a non-rotating star can only have polar fluid modes (cf section 5.2.1), the w-modes occur as polar or axial parity modes, just as in the case of black holes. Axial w-modes of a neutron star can be determined from a single scalar wave equation with a potential, in complete analogy to quasinormal modes of a black hole.

The different families of w-modes and their properties can be summarized as follows.

- Standard w-modes, or curvature modes. There appears to be an infinite number of them, the lowest frequency is of the order of 10 kHz (roughly 6–12 kHz, depending on the equation of state), with a damping time of the order of a few tenths of a millisecond. Their frequencies increase monotonically with the order of the mode; the damping rate increases monotonically as well, but at a slower rate.
- w_{II}-modes, or interface modes, can be regarded as similar to waves scattered off a sphere [104]. There is only a finite number of them, e.g. two for a typical neutron star or three for a very compact star. Their frequencies are usually somewhat lower and their damping stronger than for the standard w-modes.
- Trapped modes occur only for ultracompact stars, there is no realistic equation of state allowing such stars to exist. Their number is finite, with more compact stars showing more of them. Actually, trapped modes can be regarded simply as limiting cases of standard w-modes for increasing compactness of the star, as Andersson *et al* [104] have demonstrated for uniform density stars. Axial trapped modes were first studied by Chandrasekhar and Ferrari [64], both axial and polar trapped modes can be found in [49, 104].

6.13. Influence of the properties of the stellar fluid

Leins *et al* [45] studied the behaviour of the w- and w_{II}-modes as the star is made more compact by increasing its central density as well as changing the polytropic index in the equation of state. They found a distinct behaviour for frequencies belonging to either family of modes. None of them, however, approach the quasinormal frequencies of a black hole if the star is made as compact as general relativity allows, with the star's Schwarzschild radius approaching $\frac{8}{9}$ of

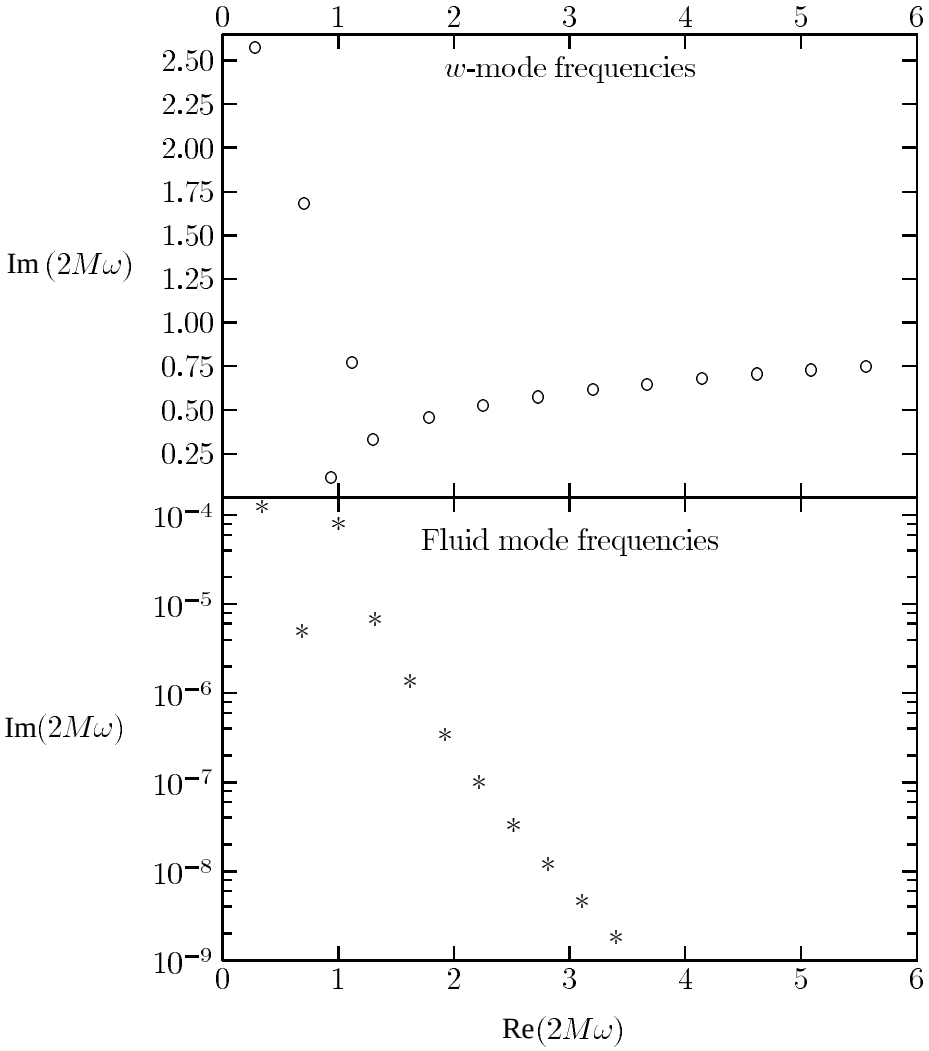

Figure 6. Complex frequencies of w-modes and fluid modes of a relativistic neutron star. The left-most frequency in the lower graph belongs to the f-mode and the others to p-modes.

its actual radius. Further studies of fluid modes and polar and axial w-modes for increasingly relativistic stars have been done by Andersson, Kokkotas and Kojima [9, 104].

Andersson and Kokkotas [9] have studied the f-mode, the first p-mode and the first standard w-mode for 12 different equations of state. They found that the f-mode and the w-mode depend only very little on the details of the equation of state. The frequency of the f-mode can be described quite accurately as a function of the average density $M_{\rm star}/R_{\rm star}^3$) of the star, and the w-mode as a function if its compactness $M_{\rm star}/R_{\rm star}$, as illustrated by figures 7 and 8. The frequency of the p-mode, on the other hand, is more sensitive to the equation of state and therefore to the details of the stellar structure.

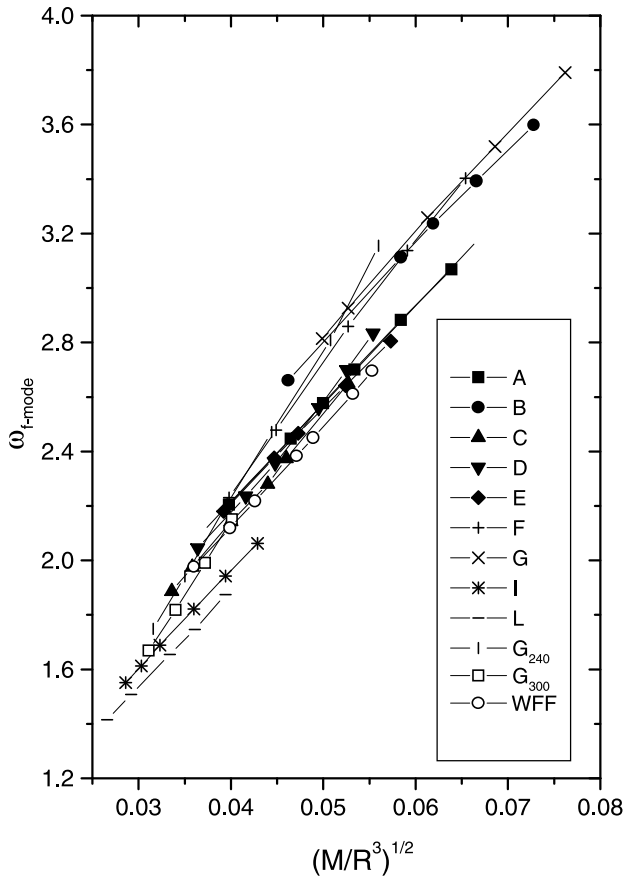

Figure 7. From [9]: frequencies of f-modes of neutron star models for different equations of state, plotted against the mean stellar density.

6.14. Topics for further reading

- Fluid modes in the Cowling approximation [105].
- w-modes in the inverse Cowling approximation [106].
- Fluid modes with more realistic physics [107].
- Fluid modes for many different equations of states [101].
- Model problems and analogies [47, 48, 108, 109].
- Modes of increasingly compact stars [110, 111].

7. Quantifying the excitation of quasinormal modes

With all the tools we now have available, it is surprising that we still cannot answer the following simple question: how strongly is a given quasinormal mode excited, either as determined by given initial data, or determined by the time evolution of the perturbation following from this initial data?

When we talk about the strength of excitation, we do not simply refer to the determination of the coefficients in the mode sum (63). Rather, we want to discuss questions such as these:

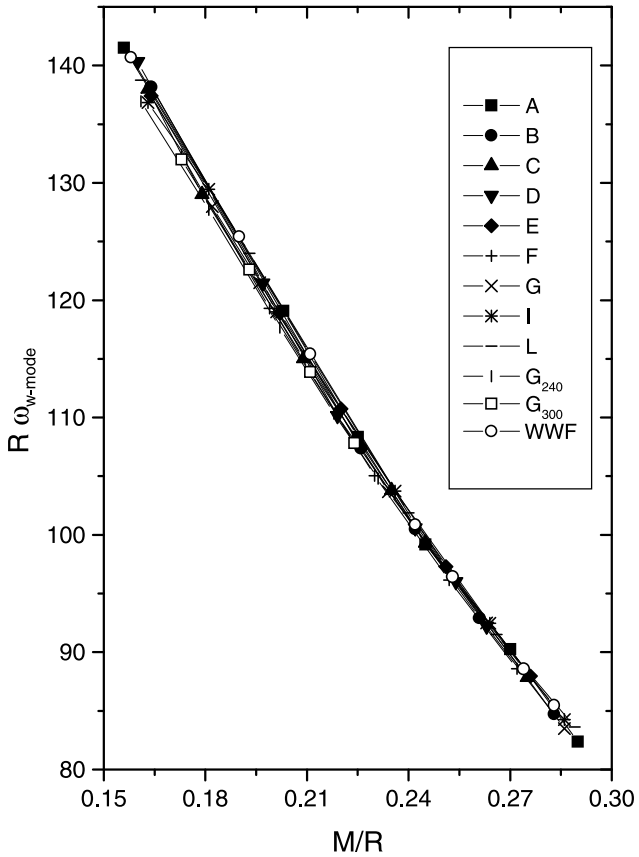

Figure 8. From [9]: frequencies of w-modes of neutron star models for different equations of state, plotted against the compactness of the star.

is a given mode excited more strongly by one set of initial data, or one physical process, compared to another? What fraction of the energy of a given gravitational wave is contained in the fundamental quasinormal mode? It turns out that answering these questions is quite a different task from expanding a wave form in terms of quasinormal modes as it was discussed in section 4.

7.1. The time-shift problem

Why can we not simply use the coefficients of the sum in equation (63) as the measure for the excitation? The magnitude of the quasinormal wavefunction decays with time, and therefore the coefficients depend on the zero point in time that one chooses. In other words, if the same signal occurs at a later time (relative to the chosen zero point), it will have larger coefficients than the identical signal occurring at an earlier time (see figure 9). This is clearly not a good way to quantify the excitation of quasinormal modes.

We might attempt to align signals on the time axis before determining, and comparing, their excitation coefficients. This will work for signals which are similar enough to allow such an alignment. However, if the two signals have a rather different structure (as shown in

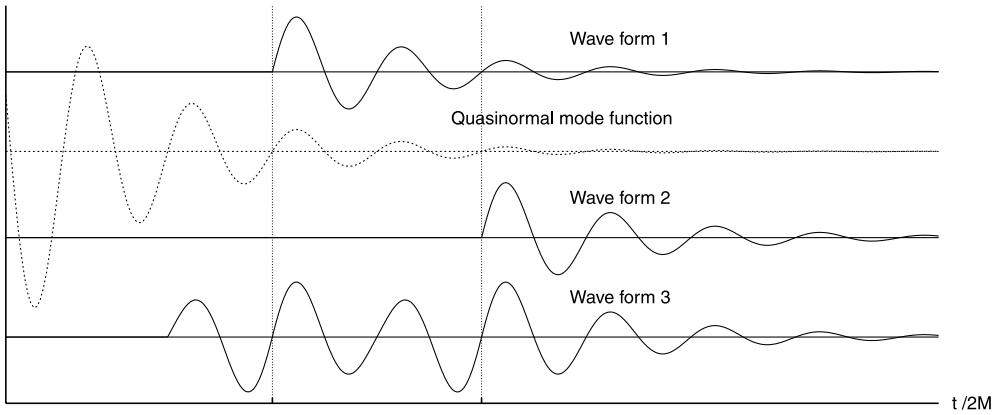

Figure 9. The time-shift problem: the zero point in time influences the coefficients in a quasinormal-mode sum for a wave form. The second graph (dotted curve) shows the fundamental quasinormal-mode function, the other graphs are examples of different wave forms to be represented as sums over quasinormal modes.

the last graph of figure 9), the alignment becomes rather arbitrary. Once again, a meaningful comparison of mode coefficients will not be possible.

7.2. Adding up energies

Maybe we should not be so concerned with the coefficients in the mode sum—after all, what we are really interested in is the energy contained in the quasinormal modes, or a specific mode, versus the total energy of a gravitational wave signal. Why not look at the energy contained in each of the pairs of quasinormal modes in the sum of equation (63)?

Again, we run into a problem: if we compute the energies corresponding to all complex conjugate pairs of modes, we find that they do not add up to the total energy of the signal, even in cases where no tail is present [112]. In particular, the energy of the fundamental mode contribution alone can be higher than the total energy of the signal. Looking at the example of the close limit approximation for two initially stationary black holes again, figure 10 makes it immediately obvious that the energy in the first-mode contribution exceeds the total energy of the signal.

In normal-mode systems, we are used to the energies of the modes adding up to the total energy. Once again, this is a helpful consequence of the fact that normal modes of a self-adjoint system form a complete, orthonormal system. Quasinormal-mode sets, on the other hand, are generally not complete. Even if we have a problem where they are, the modes are usually not orthogonal to each other. In fact, there is no known system with an orthogonal set of quasinormal modes.

Of course, when we talk about orthogonality, we need a scalar product first. Leung *et al* [40] have defined a scalar product which allows a set of quasinormal modes to be orthogonal. However, it is not a scalar product in the strict mathematical sense, since it is not positive definite. Unfortunately, it also does not allow us to assign each pair of quasinormal modes a unique energy in such a way that the energies of all pairs of modes add up to the total energy of the signal. In order to allow that, the modes would need to be orthogonal under a scalar product which is related to the expression for the energy of a gravitational wave. We will discuss such a scalar product in the next section.

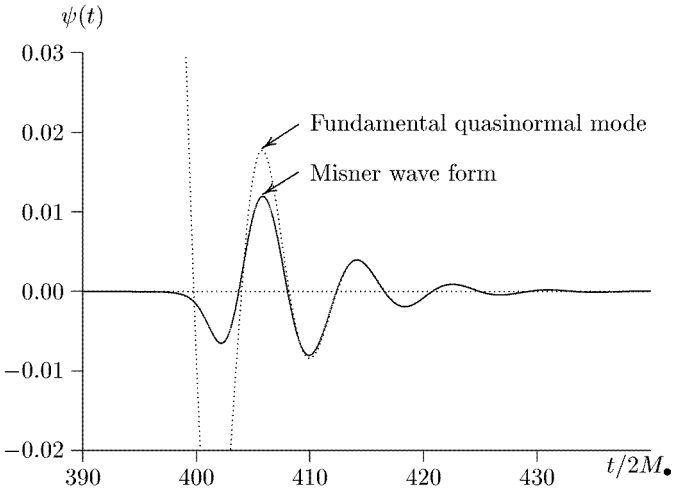

Figure 10. Gravitational radiation from the head-on collision of two black holes and the contribution of the fundamental quasinormal mode to the mode sum.

7.3. Non-orthogonal basis

Since the lack of orthogonality between the quasinormal modes presents such an unpleasant problem, Nollert and Price [37] have suggested using a formalism that is adapted to this property. They assume a complete set of quasinormal modes, either as an intrinsic property, or after some modification of the problem. The quasinormal modes then form a non-orthogonal basis of the vector space of solutions of the differential equation.

The coefficients in the mode sum can then be regarded as the *contravariant* coefficients of the solution vectors. In this vector space, define a scalar product by

$$\langle \Phi, \Psi \rangle = \int_{t_{\min}}^{\infty} \Phi^*(t, x)\Psi(t, x)\,\mathrm{d}t, \tag{97}$$

where $t_{\min}$ is the earliest time that the signal can reach the observer (cf figure 3). If the signal originates from initial data with compact support such that the perturbation vanishes initially for all $x \geqslant x_1$, then $t_{\min} = x_{\text{obs}} - x_{\text{r}}$.

Based on this scalar product, a metric for this non-orthogonal basis is given by

$$G_{kj} = \langle u_k, u_j \rangle. \tag{98}$$

This metric is Hermitian, i.e. $G_{jk} = G^*_{kj}$ for all j, k.

The covariant coefficients of the signal Ψ with respect to the basis $\{u_k\}$ are then given by

$$c_k = \langle u_k, \Psi \rangle = G_{kj}c^j. \tag{99}$$

Define an excitation coefficient by

$$\epsilon_j := c^{*j}c_j. \tag{100}$$

There is no summation implied on the right-hand side of this definition; it is just the product between the complex conjugate of the contravariant coefficient and the covariant coefficient.

It is easy to see that the excitation coefficient defined in this way is independent of the chosen zero point in time, i.e. the time-shift problem has disappeared. It is therefore a much

better quantity to characterize the excitation than the contravariant coefficients in the mode sum.

The excitation coefficient has some interesting simple properties. If Ψ describes an axial perturbation of a Schwarzschild spacetime, then the total energy of the gravitational radiation produced by that perturbation is given by (cf [53, 113])

$$E = \int_{t_{\min}}^{\infty} |Q|^2 \, \mathrm{d}t = \|Q\|^2 = \sum_k c^{*k} c_k = \sum_k \epsilon_k, \tag{101}$$

i.e. simply by the sum over the excitation coefficients. On the other hand, if Ψ describes a polar perturbation, then its energy is given by

$$E = \int_{t_{\min}}^{\infty} \left|\dot{Z}\right|^2 \mathrm{d}t = \|\dot{Z}\|^2 = \sum_k \left(\omega_k^*\right)^2 c^{*k} c_k = \sum_k \left(\omega_k^*\right)^2 \epsilon_k. \tag{102}$$

Again, all these sums are real because the quasinormal modes come in complex conjugate pairs.

The covariant coefficients can also be written as

$$c_k = \langle u_k, \Psi \rangle = \int_{t_{\min}}^{\infty} u_k^* \Psi \, \mathrm{d}t, \tag{103}$$

with the contravariant ones obtained from them via

$$c^j = \langle u_j, \Psi \rangle = G^{jk} c_k, \tag{104}$$

where the matrix G^{jk} denotes the inverse of G_{jk}.

This means that we can play this game in both directions: in a 'theoretical' calculation, starting with initial data, we may determine the contravariant coefficients via the Green's function and the covariant ones from equation (99). On the other hand, if we want to analyse a signal that has been obtained 'experimentally', we may determine the covariant coefficients from equation (103) and then use equation (104) to find the contravariant ones.

However, this definition of the excitation strength has a major drawback: the contributions to the sums in equations (101) and (102) are not guaranteed to be positive. In fact, they quite often turn out to be negative [37]! Conversely, contributions arising from individual pairs of quasinormal modes may be larger than the sum itself. We can draw the conclusion that this method of defining quasinormal-mode excitations provides us with an unambiguous way of characterizing the excitation of each mode, but it still does not allow us to quantify the excitation of an individual mode, or compare excitations between different signals in a quantitative way.

7.4. Orthogonal projection

Rephrasing the question slightly from 'how strongly are the quasinormal modes excited for a given signal?' to 'how much of the energy of a given signal is contained in a certain quasinormal mode?', Nollert [112, 114] has suggested to represent the signal Ψ as an orthogonal decomposition:

$$\Psi = \Psi_{\parallel} + \Psi_{\perp}. \tag{105}$$

$\Psi_{\parallel}$ is the part of Ψ parallel to a given quasinormal mode, while $\Psi_{\perp}$ is perpendicular to it. This decomposition is achieved using the standard procedure of orthogonal projection with equation (97) as the definition of the scalar product. More precisely, $\Psi_{\parallel}$ lies in the two-dimensional subspace spanned by a given complex conjugate pair of quasinormal modes.

Obviously, this can be extended to a projection on a subspace of any finite number of quasinormal modes that one might be interested in.

If the energy of the signal is given by the norm of Ψ under the scalar product we use, then the energy of the parallel contribution $\Psi_\parallel$ and of the orthogonal remainder $\Psi_\perp$ will obviously add up to the total energy of Ψ. This is the case for an axial perturbation of a Schwarzschild spacetime. For the polar contribution, we can modify the definition of the scalar product to

$$\langle \Phi, \Psi \rangle = \int_{t_{\min}}^{\infty} \dot{\Phi}^*(t, x)\dot{\Psi}(t, x)\, \mathrm{d}t \tag{106}$$

to preserve this property.

We have mentioned before that it is often not a good idea to start the quasinormal-mode representation of a signal at the earliest possible time. One may therefore replace $t_{\min}$ in equations (97) and (106) by some later time, making it necessary to define a method for choosing a specific time. A discussion of this aspect can be found in [112, 114].

It is now meaningful to make statements such as 'X per cent of the energy in this signal is contained in the first two quasinormal modes' or 'this signal excites the first quasinormal mode Y times as much as another signal', the quantity we refer to as the energy of $\Psi_\parallel$ in equation (105).

On the other hand, if we compute separate projections onto each quasinormal mode, the energies of these individual projections will not add up to the total energy of the signal. In fact, since the projections are not identical to the corresponding contributions in the mode sum (63), the projections themselves will not add up to the total signal, either. This difficulty is an unavoidable consequence of the fact that the quasinormal modes do not form an orthogonal set; therefore, there is no way to remedy this problem.

Note that we do not need to know here whether the quasinormal modes form a basis for the solutions we are studying. We are only interested in the part of a given signal that is described by a (finite) number of quasinormal modes, and some kind of orthogonal remainder. This remainder can include contributions from a (potentially infinite) number of quasinormal modes not included in the set we have chosen, but it can also include contributions not described by quasinormal modes at all, such as tails.

Using this approach on gravitational radiation produced by the head-on collision of two black holes, Nollert [112] finds that 82% of the energy is radiated in the fundamental quasinormal mode.

7.5. Topics for further reading

- Excitation of quasinormal modes of a black hole:
  - ∗ by particles falling into or orbiting a black hole [73, 115, 116];
  - ∗ by dust collapse [53];
  - ∗ by the collision of two black holes [8];
  - ∗ obtained from fully nonlinear computations [7, 117].

8. Analysing gravitational waves using quasinormal modes

Many authors have verified the existence of quasinormal modes for various systems under study. Relatively few have actually attempted to extract quasinormal frequencies from time-evolved data, as discussed in section 6.2. Moreover, the question of extracting quasinormal frequencies from measured gravitational waves has only been studied fairly recently [118–120],

with the prospect of a new generation of gravitational wave detectors becoming operational in the near future.

These detectors will hopefully observe gravitational waves originating from black holes and neutron stars. Analysing these waves in terms of quasinormal modes could provide a wealth of information: the frequencies of the modes depend on the masses of the objects, and in the case of neutron stars, on their radii as well. This could provide a direct confirmation for the existence of a black hole. Knowing the mass and radius of a neutron star could set extremely valuable constraints on its equation of state [118].

We mention in passing that the f-mode with a frequency of about 2 kHz is still close to the sensitivity range of the interferometric detectors, while the first p-mode (several kHz) and quasinormal modes of black holes as well as w-modes of neutron stars, with frequencies of typically 10 kHz and higher, might require the recently suggested spherical resonant mass detectors [121] tuned to sufficiently high frequencies.

8.1. Identifying a signal

Before we can analyse a wave form, we have to identify it in the detector output and extract it from the signal. This is a very difficult task, since the actual gravitational wave signal will be buried in noise originating in the detector as well as seismic noise or background noise from astrophysical sources. Discussions of various noise sources and the sensitivity of detectors as a function of the signal's frequency can be found, for example, in [122, 123].

Identifying and extracting a signal from the noise is done using statistical methods which assess the probability that a signal is present in a given detector output. There are techniques which require templates of the expected signal; others work without templates and can be used to search for arbitrary signals, but they are more likely to miss a signal or to give a 'false alarm'. The interested reader will find detailed discussions in [124, 125] and references therein.

We will not discuss these steps any further here, since they are not specifically related to quasinormal modes. In the following, we will simply assume that we have identified a signal in the detector output, and that this signal is essentially free from noise. In fact, since no gravitational wave has been observed until now, we will have to use data from model calculations throughout the rest of this section.

8.2. QNM of black holes

The usual procedure for finding resonant frequencies in a signal is by using a Fourier transform on the signal and looking for distinct maxima in the spectrum. While this works well for undamped or slowly damped modes, the strong damping of the quasinormal modes of a black hole leads to very broad peaks in the spectrum, making it very difficult to obtain an accurate value for the real part of any frequency. In principle, the imaginary part can be related to the width of the peak, but again, we will obtain only a rough estimate.

We should therefore use a technique which is better adapted to quasinormal wave forms, such as matched filtering [126] (chapter IV.2). For studying the process of extracting information from a signal, rather than the identification of the signal buried in noise, Nollert [114] has used the orthogonal projection of the signal onto quasinormal-mode subspaces described in section 7 as a somewhat simpler alternative. The energy contained in a quasinormal mode of some (complex) frequency ω is determined, varying ω over some reasonable range and plotting the results as a function of ω. Any distinct maximum in this energy fraction indicates a resonant frequency in the signal.

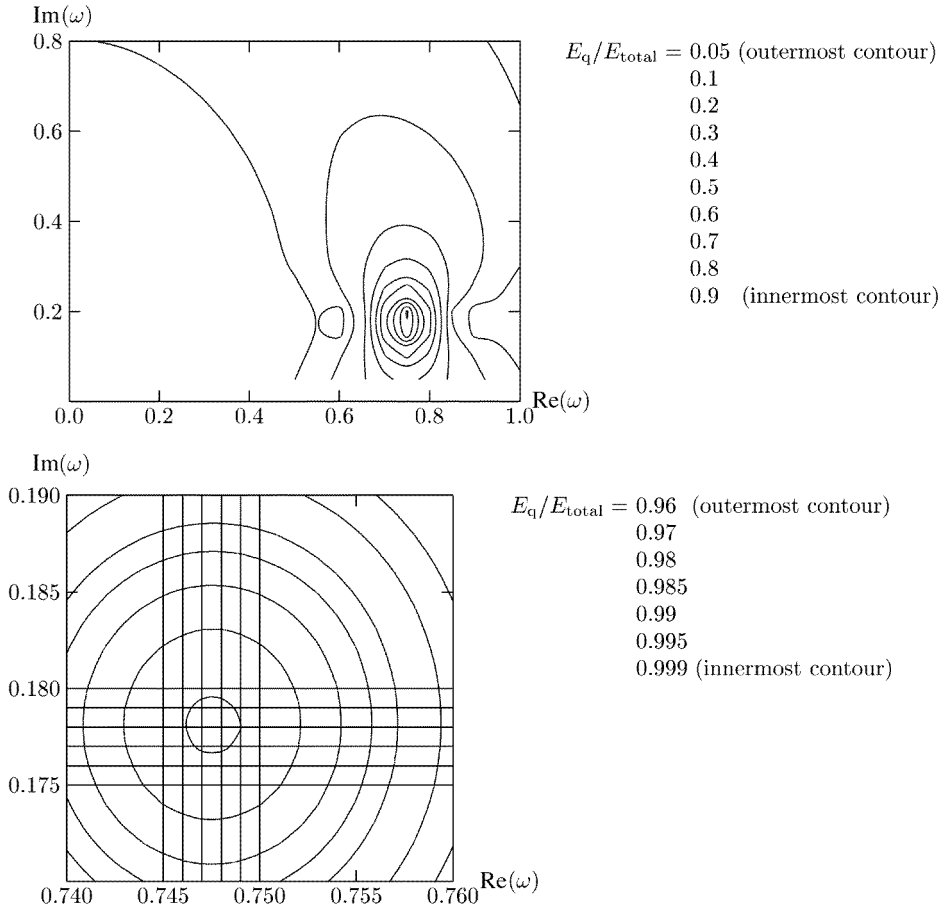

Figure 11. 'Complex' spectrum of gravitational radiation from the final black hole formed in a head-on collision of two black holes. The picture at the bottom is an excerpt of the one at the top.

This procedure is somewhat analogous to obtaining a spectrum via a Fourier transform of a signal: here, one performs a Fourier transform of a signal over a range of frequencies, plotting the amplitude of a harmonic wave at each frequency. The amplitude essentially describes the energy contained in the contribution to the total signal at this particular frequency. Any definitive maximum in the spectrum can then be regarded as a resonant frequency of the source that emitted the signal.

As we have seen before (figure 2), the quasinormal ringing is limited in the beginning by the initial pulse, and towards late times by the power-law tail. It is possible to extend the frequency analysis over the whole signal and just look for maximum energy in a quasinormal-mode wave form. However, more accurate results can be obtained if we only analyse that part of the signal which is clearly not influenced by either the initial pulse or the power-law tail.

Since quasinormal frequencies are complex, the energy fraction in the quasinormal-mode wave form is a function of two parameters. Figure 11 shows this function as a contour plot, where the part of the signal being analysed extends from $t/2M_\bullet = 421$ to 469. We clearly find

a maximum around $\mathrm{Re}(2M_\bullet\omega) = 0.75$ and $\mathrm{Im}(2M_\bullet\omega) = 0.18$. From the enlargement of this area, we read off $2M_\bullet\omega = (0.7475, 0.178)$, which is in excellent agreement with the expected value of $2M_\bullet\omega = (0.747\,34\ldots, 0.177\,92\ldots)$.

Contrary to what we expect from a Fourier spectrum, there is no evidence in figure 11 for any quasinormal frequency other than the fundamental one. The reason is that the more strongly damped modes decay too quickly to leave a signature sufficient for identifying them. However, if the contribution of the fundamental mode is subtracted from the data, the remainder will usually show evidence of the next quasinormal mode, and so on [53].

In the case of an actual detection, we would use the value extracted from the data to determine the parameters of the black hole that emitted the signal. For a Schwarzschild black hole, the frequency simply scales with the mass of the black hole. For a rotating black hole we can, in principle, obtain both its total mass and angular momentum, since the frequency consists of two independent parameters as well. In practice, however, this would probably leave us with a rather large uncertainty for both parameters.

8.3. f- and p-modes of neutron stars

Figure 12 shows gravitational waves emitted by a neutron star after it has been hit by a narrow gravitational wavepacket (top graph) or after an initial fluid perturbation (bottom graph) (see Allen *et al* [59] for similar results). The neutron star is assumed to consist of a perfect fluid with a polytropic equation of state with a polytropic index of $n = 1$ and $K = 100\ \mathrm{km}^{-2}$. The central density is $3 \times 10^{15}\ \mathrm{g\ cm}^{-3}$, resulting in a total mass of $M_{\mathrm{star}} = 1.266M_\odot$ and a radius of $R_{\mathrm{star}} = 8.862$ km, or $R_{\mathrm{star}}/2M_{\mathrm{star}} = 2.37$. The wavepacket impinging on it initially consist of a Gaussian with a full width at half maximum of 5.27 km, i.e. only about half the radius of the star. The fluid perturbation for the second wave form is shaped roughly like one full period of a cosine; an initial metric perturbation results from this fluid perturbation via the constraint equations. Figure 12 shows the initial pulse, followed by w-mode ringing, which is overtaken by f- and p- mode ringing later.

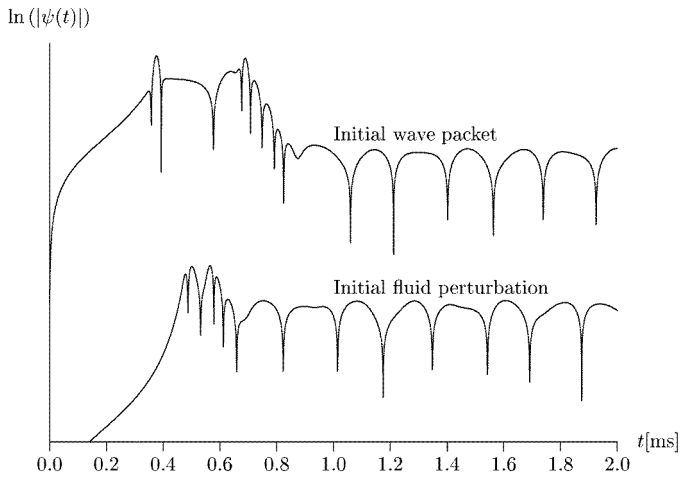

Figure 12. Gravitational wave forms generated by a Gaussian wavepacket hitting a neutron star (top graph) and by an initial fluid perturbation (bottom graph). Scaling of the graphs is arbitrary and has been chosen for convenience.

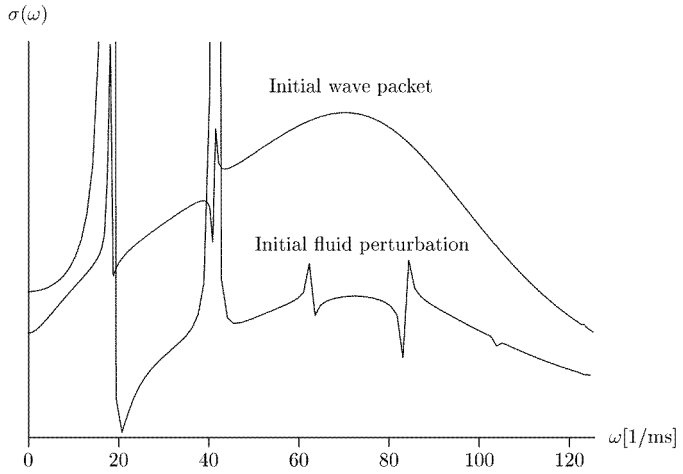

Figure 13. Fourier transform of the wave forms in figure 12. Scaling of the graphs is arbitrary and has been chosen for convenience.

Figure 13 shows the Fourier spectrum obtained from analysing these signals in their entirety. The broad peak corresponds to the fundamental w-mode of the neutron star. The two sharp peaks which are easily visible belong to the f-mode and the first p-mode. If the time range dominated by the initial pulse and the w-mode ringing is excluded from the Fourier analysis, the higher p-modes become more visible, and about 25 p-modes can be identified in the spectrum.

The oscillation frequencies can be read off as $\omega \approx 18\,060\ \mathrm{s}^{-1}$ ($\nu = \omega/2\pi \approx 2875$ Hz) for the f-mode and $\omega \approx 41\,220\ \mathrm{s}^{-1}$ ($\nu \approx 6560$ Hz) for the first p-mode. A stationary mode calculation yields frequencies $\omega = 18\,042\ \mathrm{s}^{-1}$ ($\nu = 2871$ Hz) for the f-mode and $\omega = 41\,175\ \mathrm{s}^{-1}$ ($\nu = 6553$ Hz) for the first p-mode of this stellar model. Since these modes are so slowly damped, we need a long stretch of data to determine the damping, i.e. the imaginary parts of the frequencies, with any reliability. However, the amount of data produced in this kind of simulation is limited by available computer resources [59]. Therefore, the determination of the imaginary parts cannot be tested using simulated data. This limitation should not apply to the analysis of actual data; in fact, measuring the signal over a long period of time will likely be a prerequisite for identifying it at all.

8.4. w-modes of neutron stars

Kokkotas *et al* [120] present a statistical analysis of the errors expected when the frequency of the fundamental w-mode is extracted from observed gravitational radiation from a neutron star. Assuming a frequency of about 10 kHz, a damping time of about 0.02 ms, and a distance to the source of only 10 kpc (within our own galaxy), the mode would have to radiate more than one solar mass as gravitational radiation in order to allow us to determine its oscillation frequency with an error of 1%, using first-generation LIGO for the detection.

The frequency of a fluid mode can be determined with a much smaller error, owing to the longer damping time. In order to determine the frequency of the f-mode or a p-mode to the same accuracy under the same conditions, the mode needs only of the order of 10^{-8} to 10^{-10} solar masses in energy. Conversely, an event radiating more energy could happen at a correspondingly larger distance, increasing the number of events available for analysis.

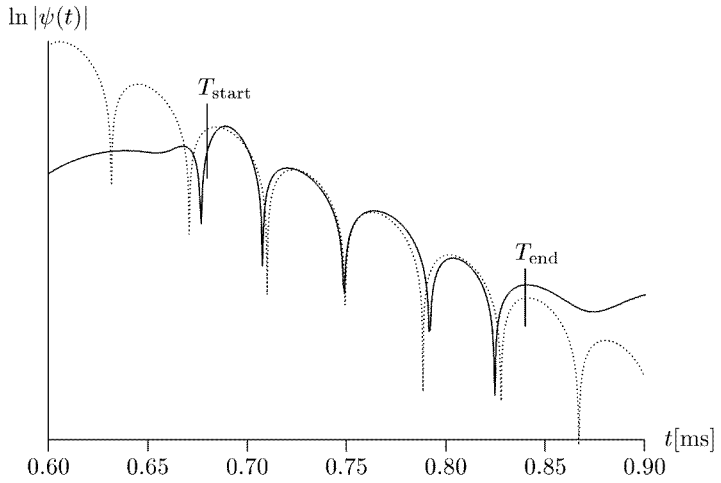

Figure 14. Gravitational wave form generated by a Gaussian wavepacket (5 km FWHM) hitting a neutron star, projected onto a w-mode with frequency $\omega = (80.1, 44.0)$ (ms)$^{-1}$.

Kokkotas *et al* [120] therefore suggest a modified scheme using the oscillation frequencies of the f-mode and the first p-mode to obtain restrictions on the equation of state and the parameters of the star.

On the other hand, assuming an advanced detector with its optimum sensitivity near the frequency of w-modes, and allowing an error of 10%, the required energy reduces to about 10^{-5} solar masses. It is therefore not completely out of the question that at some time in the future, a w-mode could be identified and its frequency determined from observed gravitational wave data.

These results are based on a simple $e^{i\omega t}$ template for the w-mode. However, figure 12 shows that interference with the initial pulse at early times and with f- and p-mode ringing at late times could disturb the appearance of the w-mode enough that it might be difficult to recognize in the signal. Nollert [114] finds that in order to determine its frequency with an error of about 5%, the w-mode should be clearly visible for at least about 1.5–2 full oscillation periods. For the signal generated by a Gaussian wavepacket with 5 km full width at half maximum hitting the star, they find that a projection onto a w-mode with a frequency of $\omega = (80.1, 44.0)$ (ms)$^{-1}$, as shown in figure 14, provides the best representation of the signal. The time window used for the projection is indicated by vertical bars in figure 14. A detailed analysis results in a possible range of $\mathrm{Re}(\omega) = 75$–84 (ms)$^{-1}$ and $\mathrm{Im}(\omega) = 39$–45 (ms)$^{-1}$. A time-independent calculation [45] yields $\omega = (80.7, 42.4)$ (ms)$^{-1}$ for the fundamental w-mode of this stellar model.

The initial fluid perturbation leads to a shorter stretch of visible w-mode ringing in the signal. Also, it is not clear how much of it is disturbed by interference with the initial pulse and with the f- and p-mode contributions. Figure 15 shows two possible projections of this signal onto w-modes with frequencies $\omega = (67.8, 39.6)$ (ms)$^{-1}$ (upper graph) and $\omega = (84.4, 40.4)$ (ms)$^{-1}$ (lower graph). Note that the upper projection results in an apparently better fit of the data, but its frequency is much further from the correct value than the one for the projection in the lower graph. Altogether, this signal admits a range of w-mode frequencies of about $\mathrm{Re}(\omega) = 62$–94 (ms)$^{-1}$ and $\mathrm{Im}(\omega) = 32$–44 (ms)$^{-1}$.

Nollert concludes that sufficient total energy in the w-mode is only one prerequisite for an accurate determination of its frequency. In addition, the overall shape of the signal, and

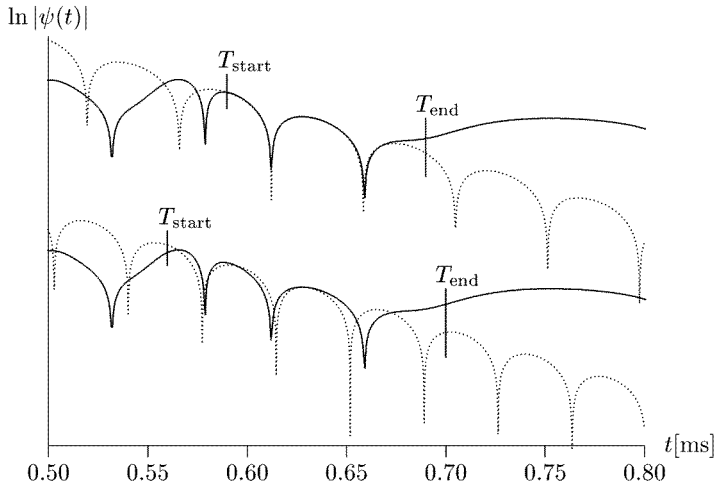

Figure 15. Gravitational wave form generated by an initial fluid perturbation, projected onto w-modes with frequencies $\omega = (67.8, 39.6)$ (ms)$^{-1}$ (upper graph) and $\omega = (84.4, 40.4)$ (ms)$^{-1}$ (lower graph). Scaling of the graphs is arbitrary and has been chosen for convenience.

by implication, the properties of the initial perturbation, must allow the w-mode component to dominate the signal for a sufficiently long stretch of time. As a general rule, wider initial gravitational wave pulses generate less w-mode ringing than narrower ones, and less relativistic stars show less w-mode ringing than more relativistic ones. An initial fluid perturbation tends to produce more f- and p-mode and less excitation of the w-mode. If the initial metric perturbation resulting from the fluid displacement is chosen to be conformally flat (unlike the example shown in figure 12), then the fluid modes tend to completely cover up the w-mode component.

In fact, most astrophysical events which can give rise to oscillations of a neutron star (such as a collapse, starquakes, objects hitting the star or collisions) will involve strong fluid perturbations. Model calculations for a particle scattered by a neutron star [127–130] only show evidence of w-mode ringing for an ultracompact star (too compact for any realistic equation of state) or for an extremely relativistic particle passing so close to the star that it almost grazes its surface. A calculation for the late stage of a binary neutron star merger [131] shows only excitations of the fluid modes. However, this dominance of the fluid modes depends strongly on the way in which the initial data are determined: it is most prominent if the assumption is used that the initial spatial slice is conformally flat, in analogy with the procedure frequently used to obtain initial data for the time evolution of black holes [132]. If this assumption is abandoned, then different initial data for the metric perturbation can be found—while keeping the initial fluid perturbation the same—which will excite visible w-mode ringing. One could argue that this corresponds to artificially putting extra gravitational radiation into the initial slice. Keep in mind, however, that there is no way to decide which part of any initial gravitational radiation is artificial, and which part is natural to the system under study, unless one computes the history of this system from a point where the physical meaning of all parts is well understood. Usually, this means starting with the components of the system being asymptotically far apart.

An astrophysical scenario which might come close to producing the desired w-mode excitation could be a collapsing neutron star or black hole binary, emitting a strong, sharp gravitational wave pulse which, in turn, excites perturbations of a nearby neutron star. However,

no model calculations exist at present to give us an idea if such a scenario might work, or how often we could expect it to happen.

8.5. Information obtained from a quasinormal-mode spectrum

For a Schwarzschild black hole, the only parameter involved is its mass $M_\bullet$. The quasinormal frequencies scale with the mass and therefore provide a direct measure for it. For a rotating black hole, a second parameter is the angular momentum. The quasinormal spectrum as a function of mass and angular momentum is well known [84], and if one or two frequencies are known with sufficient accuracy, both parameters can be determined directly from this relationship.

The situation is much more complicated for neutron stars. For one thing, a neutron star has a much more complicated structure than a black hole. Even if we neglect the influence of this structure on the frequencies, making the much simplified assumption that the star consists of a perfect fluid throughout, then we are still facing the influence of the equation of state on the star, and therefore on its spectrum of oscillations.

On the other hand, it would be extremely valuable if this influence could be used to obtain information about the equation of state from a measured spectrum of neutron star oscillations. In principle, one could calculate a theoretical spectrum for a variety of potential equations of state and then compare them with an experimentally determined spectrum. However, in practice the spectrum will probably not be distinct enough to provide a clear decision for one particular equation of state among the many candidates that exist.

A more systematic approach has been suggested by Andersson and Kokkotas [9]. They start by relating the spectrum to the fundamental parameters of the star, its total mass and its radius. This is possible via the scaling relations for the real parts of the f-mode and the fundamental w-mode discussed in section 6.13. Fitting all curves in figure 7 to a single smooth line provides an approximate relationship between the frequency of the f-mode and the average density of the star $M_{\rm star}/R_{\rm star}^3$. Another relationship between the frequency of the fundamental w-mode and the compactness of the star $M_{\rm star}/R_{\rm star}$ is obtained likewise from figure 8. Conversely, if the frequency of the f-mode can be extracted from observation, we can use this relationship to determine an approximate value for $M_{\rm star}/R_{\rm star}^3$, and the frequency of the w-mode provides an approximate value for $M_{\rm star}/R_{\rm star}$. With both of these, $M_{\rm star}$ and $R_{\rm star}$ can both be determined individually.

Any given equation of state allows a certain maximum mass and minimum radius for a neutron star. Therefore, knowing the values of these parameters would be very valuable in placing constraints on potential equations of state. There are currently very few observations providing information on both $M_{\rm star}$ and $R_{\rm star}$, indicating that a mass of $1.45M_\odot$ must be allowed by a realistic equation of state. Observation of an isolated neutron star by the Hubble space telescope [133] shows a radius of 14 km or less. In order to tighten these constraints significantly, we can probably not allow an error of more than about 5–10% for the determination of $M_{\rm star}$ and $R_{\rm star}$. Following Kokkotas *et al* [120], this requires a 2.5–5% accuracy for the frequencies extracted from the data.

We have discussed in the previous section why it is unlikely that the frequency of the fundamental w-mode will be measured with the required accuracy any time soon. Therefore, Kokkotas *et al* [120] have suggested an alternative, involving the frequencies of the f-mode and the first p-mode. Using the f-mode frequency, a value for the mean stellar density, $M_{\rm star}/R_{\rm star}^3$, is determined. Plotting the p-mode frequency as a function of $M_{\rm star}/R_{\rm star}^3$ for a sample of equations of state will not yield a simple dependence. Nevertheless, the value of $M_{\rm star}/R_{\rm star}^3$ obtained from the f-mode frequency together with the measured p-mode frequency

will fix a point on this plot. Somewhere near this point, there should be a candidate (or possibly several of them) for a p-mode frequency for some equation of state. This equation of state is then singled out as the 'most likely' one. The mass and radius of the star are computed by solving the TOV equations with this particular equation of state.

Despite the difficulties we have described in the previous section, there is the exciting promise that a quasinormal-mode analysis of observed gravitational radiation from black holes and neutron stars can provide extremely valuable information on these objects, their inner structure and the nuclear equation of state at very high densities.

8.6. Topics for further reading

- A review on gravitational waves, their detection and their significance for astrophysics [134].
- Signal extraction and analysis [135, 136].
- Computational requirements for data analysis [137].
- Resonant excitation of fluid modes by an orbiting particle [138].

Acknowledgments

We are grateful to N Andersson, B Schmidt and U Kraus for discussions clarifying many aspects of this topic. We also thank R Price, P Laguna, K Kokkotas, W Krivan and M Kunle for carefully reading the manuscript and providing numerous suggestions for improvement.

Appendix. Quasinormal modes of rotating black holes and neutron stars

Astrophysical black holes and neutron stars will almost certainly possess angular momentum. While the basic concept of quasinormal modes does not change when applied to rotating objects, there are many new technical issues and problems. In addition, new physics enters the picture, such as super-radiance for rotating black holes or unstable modes for rotating neutron stars. This summary is extremely brief; more details on quasinormal modes of black holes have been given by Kokkotas and Schmidt [139] and an extensive review on rotating stars in general relativity by Stergioulas [69].

A.1. Rotating black hole background

A rotating black hole carrying angular momentum is described by the Kerr metric [55]:

$$\mathrm{d}s^2 = \frac{\Delta}{\rho^2}\left[\mathrm{d}t - a\sin^2\theta\,\mathrm{d}\varphi\right]^2 + \frac{\sin^2\theta}{\rho^2}\left[(r^2+a^2)\,\mathrm{d}\varphi - a\,\mathrm{d}t\right]^2 + \frac{\rho^2}{\Delta}\,\mathrm{d}r^2 + \rho^2\,\mathrm{d}\theta^2, \tag{A1}$$

where a is the angular momentum parameter ($0 \leqslant a \leqslant M_\bullet$), (t, r, θ, φ) are the standard Boyer–Lindquist coordinates, and

$$\Delta = r^2 - 2M_\bullet r + a^2 \qquad \rho^2 = r^2 + a^2\cos^2\theta. \tag{A2}$$

While the Schwarzschild metric is the unique spherically symmetric vacuum solution of the Einstein equations, the Kerr metric is not the only axisymmetric vacuum solution. The geometry in the empty space surrounding axisymmetric rotating stars is not a Kerr geometry. In fact, there is no known material source which could be matched to a general exterior Kerr spacetime.

A.2. Perturbations of a Kerr geometry

The approach of studying metric perturbations directly, as described in section 2 for perturbations of the Schwarzschild metric, leads to gauge-dependent results for a Kerr background. Using the Newman–Penrose formalism as an alternative, Teukolsky [140] derived a master equation covering not only gravitational perturbations, but scalar, two-component neutrino and electromagnetic fields as well. Using Boyer–Lindquist coordinates and the Kinnersley null tetrad, this master evolution equation reads

$$-\left[\frac{(r^2+a^2)^2}{\Delta}-a^2\sin^2\theta\right]\partial_{tt}\Psi-\frac{4M_\bullet ar}{\Delta}\partial_{t\varphi}\Psi-2s\left[r-\frac{M_\bullet(r^2-a^2)}{\Delta}+\mathrm{i}a\cos\theta\right]\partial_t\Psi$$
$$+\Delta^{-s}\partial_{\mathrm{r}}\left(\Delta^{s+1}\partial_{\mathrm{r}}\Psi\right)+\frac{1}{\sin\theta}\partial_\theta(\sin\theta\,\partial_\theta\Psi)+\left[\frac{1}{\sin^2\theta}-\frac{a^2}{\Delta}\right]\partial_{\varphi\varphi}\Psi$$
$$+2s\left[\frac{a(r-M_\bullet)}{\Delta}+\frac{\mathrm{i}\cos\theta}{\sin^2\theta}\right]\partial_\varphi\Psi-\left(s^2\cot^2\theta-s\right)\Psi=0, \tag{A3}$$

where s is the spin weight ($s=\pm2$ for gravitational perturbations, $s=0$ for scalar waves). For gravitational perturbations, the function Ψ is given in terms of the Weyl tensor tetrad components ψ_0 and ψ_4: $\Psi=\psi_0$ for $s=+2$ and $\Psi=\rho^{-4}\psi_4$ for $s=-2$, with $\rho=-1/(r-\mathrm{i}a\cos\theta)$.

The angular variable φ can be separated in the usual way, but in the time domain, a separation of θ is not possible. While a numerical integration in (2 + 1) dimensions of equation (A3) might appear straightforward, there are considerable technical problems to overcome. Krivan *et al* [141] developed a code to study the scalar wave equation and gravitational perturbations on a Kerr background. They found that the behaviour of the late-time power-law tails is unaffected by the spin of the black hole and they confirmed the quasinormal frequencies calculated via mode analysis.

Teukolsky [140] found that equation (A3) is separable in r and θ in the frequency domain: writing Ψ as

$$\Psi_{LM}(t,r,\theta,\varphi)=\frac{1}{\sqrt{2\pi}}\mathrm{e}^{\mathrm{i}\omega t}R_{LM}(r,\omega)S_{LM}(\theta,\omega)\,\mathrm{e}^{\mathrm{i}m\varphi}, \tag{A4}$$

the following equations must be satisfied by $R_{LM}(r,\omega)$ and $S_{LM}(\theta,\omega)$:

$$\Delta^{-s}\frac{\mathrm{d}}{\mathrm{d}r}\left(\Delta^{s+1}\frac{\mathrm{d}R}{\mathrm{d}r}\right)+\left[\frac{K^2-2\mathrm{i}s(r-M_\bullet)K}{\Delta}+4\mathrm{i}s\omega r-\lambda\right]R=0 \tag{A5}$$

$$\frac{1}{\sin\theta}\frac{\mathrm{d}}{\mathrm{d}\theta}\left(\sin\theta\frac{\mathrm{d}S}{\mathrm{d}\theta}\right)+\left[a^2\omega^2\cos^2\theta-\frac{m^2}{\sin^2\theta}-2a\omega s\cos\theta\right.$$
$$\left.-\frac{2ms\cos\theta}{\sin^2\theta}-s^2\cot^2\theta+E(\omega)-s^2\right]S=0, \tag{A6}$$

where $K\equiv(r^2+a^2)\omega-am$ and $\lambda\equiv E(\omega)-s(s+1)+a^2\omega^2-2am\omega$.

The angular equation (A6), together with a regularity condition at the origin, has eigenvalues $E_{LM}(\omega)$ for every value of ω, the corresponding eigenfunctions S_{LM} are called 'spin-weighted spheroidal harmonics'. Once determined from the angular equation, the separation constant E_{LM} enters the radial equation as a constant. However, since this separation depends on ω, it cannot be carried over into the time domain.

Using the radial equation (A5), quasinormal modes can be defined in analogy to quasinormal modes of the Regge–Wheeler or the Zerilli equation. They have been calculated, for example, by Detweiler [142], Leaver [84] and others [143–145].

It turns out that extremal Kerr black holes have very slowly damped (possibly undamped) quasinormal modes for $m = -l$. This leads to the effect of super-radiant scattering, where an impinging wave is amplified as it scatters off the black hole. This phenomenon was first discovered by Zel'dovich [146] and has since been discussed, for example, by Andersson *et al* [147].

A.3. Equilibrium state of rotating neutron stars

The general form of the metric of an axisymmetric spacetime is a generalization of equation (71) for spherically symmetric stars:

$$(\mathrm{d}s^2)_0 = -\mathrm{e}^{\nu(r,\theta)}\,\mathrm{d}t^2 + \mathrm{e}^{\lambda(r,\theta)}\left(\mathrm{d}r^2 + r^2\,\mathrm{d}\theta^2\right) + \mathrm{e}^{\Psi(r,\theta)}(\mathrm{d}\varphi - \omega(r,\theta)\,\mathrm{d}t)^2. \tag{A7}$$

Once again, the Einstein field equations and the equation of hydrostatic equilibrium have to be solved numerically, and again, simplifying assumptions such as a perfect fluid and zero temperature are employed to make the problem manageable. Four of the ten field equations are actually independent. The main methods for solving them are:

- Hartle's slow rotation formalism [148] limits the changes in the structure of the star to the quadrupole term, reducing the equilibrium equations to a set of ordinary differential equations.
- Butterworth and Ipser [149] use a Newton–Raphson-like scheme, starting with a non-rotating model, they increase the angular velocity in small steps, treating each new model as a linear perturbation of the previously computed one.
- Komatsu *et al* [150] convert the three elliptic field equations into an integral equation, using an appropriate Green's function to solve them; the fourth equation is an ordinary first-order differential equation.
- Based on a formalism by Neugebauer and Herlt [151], Neugebauer and Herold [152] and Wu and co-workers [153, 154] relate the field equations to the minimal surface equation in an abstract Riemannian potential space. They use finite elements and a Newton–Raphson method to solve the resulting equations.
- Bonazzola *et al* [155] use the (3 + 1) formalism to derive the field equations, resulting in four elliptic equations and solve them using a spectral method.

Stergioulas and Friedman have provided a direct comparison of several different numerical codes [156].

As a general rule, the centrifugal force results in a larger maximum mass and a larger equatorial radius of the star, as compared to a non-rotating star with the same equation of state. The maximum mass typically increases by about 15–20% and the equatorial radius by about 30–40%. This distortion causes a quadrupole moment in the gravitational field far away from the star, which can be used as a measure for the distortion caused by rotation.

A.4. Perturbations of rotating neutron stars

The perturbation equation for a rotating background star must depend on M, in addition to L, just as the Teukolsky equation (A3) depends on M. However, the metric generated by a rotating star is of Petrov type I, even in the vacuum outside the star [157]. This means

that the angular variables cannot be separated in the perturbation equation. Consequently, perturbations cannot be decomposed into contributions belonging to definite values of (L, M) which evolve separately in time.

A decomposition of the perturbation into, say, tensor spherical harmonics may, of course, still be done at any given moment in time. However, the perturbation equation will not separate for different values of (L, M). Therefore, the part of a perturbation belonging to, say, $L = 2, M = 0$ at some time will contain contributions from many, possibly infinitely many, different (L, M) at a later time. For slow rotation, it can still makes sense to think of a perturbation in terms of (L, M) contributions which evolve almost by themselves, but are weakly coupled to each other.

A.5. Quasinormal modes of rotating neutron stars

Quasinormal modes, however, may be labelled with definite values of L even it the star is rotating quickly. We simply construct a sequence of stars connecting the rotating one with a non-rotating one. We regard a mode of the rotating star as a L mode if it reduces to an L mode in the non-rotating star in the sequence. Note that this procedure cannot be used to attach a value of M to a mode, since the quasinormal modes of a non-rotating star are degenerate in M.

No exhaustive, general study of quasinormal modes of rotating stars has been done yet. Several special cases have been studied; we will summarize these briefly.

Slow rotation. Kojima [61] derived the perturbation equations in the slow-rotation limit, working in the Regge–Wheeler gauge, and computed the frequencies of $L = M$ modes for various polytropes. Each polar L-mode couples to the axial $L \pm 1$ modes and each axial mode to the polar $L \pm 1$ modes. This coupling affects the frequencies only to second order in the angular velocity of the rotation [158].

Post-Newtonian approximation. Cutler and Lindblom [159] obtained frequencies for the $L = M$ f-mode in the first post-Newtonian approximation. They derive a formula which yields the first post-Newtonian correction to the mode frequency if the first post-Newtonian stationary solution and the solution to the Newtonian perturbation equation are known, eliminating the necessity to solve the first post-Newtonian perturbation equation numerically. The first post-Newtonian correction (to the Newtonian case) reduces the effect that rotation has on the mode frequencies; this reduction can be up to 12% for the fundamental $L = M$ mode of an $n = 1.0$ polytrope with $R_{\text{star}}/2M_{\text{star}} = 2.5$.

Cowling approximation. The frequencies of fluid pulsations can be estimated by studying the fluid perturbations on a fixed background metric, i.e. the metric perturbations are set to zero in the perturbation equations [107]. Yoshida and Koshima [160] found that the relative error for the $L = 2$ f-mode is 30% for $R_{\text{star}}/2M_{\text{star}} = 10$ and 15% for $R_{\text{star}}/2M_{\text{star}} = 2.5$, decreasing with higher l. It is similar for p-modes, becoming somewhat smaller for less relativistic stars and decreasing with the radial mode number.

Zero-frequency modes. Stergioulas and Friedman solved the fully relativistic perturbation equation for zero-frequency (neutral) modes of a star with a polytropic equation of state [161]. They use a specific gauge to fix four of the ten components of the metric perturbation

and numerically solve the remaining six perturbation equations and the energy conservation equations. They find that the instability of neutral modes, which had already been observed in the post-Newtonian approximation, is strengthened by full relativity. In particular, for a polytrope with index $N = 1$, the critical angular velocity for the onset of the instability is moved away significantly from the mass-shedding limit. Furthermore, the critical polytropic index for the $l = m = 2$ bar mode instability is raised to $N_{\rm crit} < 1.3$ from $N_{\rm crit} < 0.808$ in the Newtonian case.

A.6. Unstable fluid modes of rotating neutron stars

Axial perturbations of non-rotating stars do not involve oscillations of the fluid. In other words, axial fluid modes of non-rotating stars all have zero frequency. In the rotating case, axial fluid modes with non-vanishing frequencies exist; they are therefore called r-modes.

Both polar and axial fluid modes are subject to the so-called Chandrasekhar–Friedman–Schutz (CFS) instability [162]. This instability arises if a mode carries positive angular momentum in a reference frame co-rotating with the star, but negative angular momentum in the reference frame of an asymptotic observer (or vice versa). The instability of the polar modes is subject to conditions regarding the equation of state and a minimum angular velocity of the star depending on the value of L of the mode. r-modes, on the other hand, are generically unstable: all r-modes with $L \geqslant 2$ are unstable for any value of the angular velocity of the star [163]. Their growth is eventually limited by the viscosity of the star's fluid.

The r-mode instability may be responsible for quickly reducing a neutron star's angular momentum right after it has been born [164]. This could explain why the initial rotation rates of pulsars never seem to be lower than about 10 ms. Faster millisecond pulsars, on the other hand, could be spun up by accretion at a later stage when the r-mode instability is damped strongly by viscosity.

Strong oscillations induced by the CFS instability could also turn out to be prime candidates for sources of gravitational radiation for the new gravitational wave detectors [165].

References

[1] Vishveshwara C V 1970 *Nature* **227** 936
[2] Press W H 1971 *Astrophys. J.* **170** L105
[3] Matzner R A, Seidel H E, Shapiro S L, Smarr L, Suen W-M, Teukolsky S A and Winicour J 1995 *Science* **270** 941–7
[4] Seidel E and Suen W-M 1999 *J. Computat. Appl. Math.* **109** 493–525
[5] Seidel E 1998 *Relativistic Astrophysics* ed H Riffert *et al* (Braunschweig: Vieweg) pp 229–37
[6] Abrahams A, Bernstein D, Hobill D, Seidel E and Smarr L 1992 *Phys. Rev.* D **45** 3544
[7] Anninos P, Hobill D, Seidel E, Smarr L and Suen W-M 1993 *Phys. Rev. Lett.* **71** 2851–54
[8] Price R H and Pullin J 1994 *Phys. Rev. Lett.* **72** 3297–300
[9] Andersson N and Kokkotas K D 1998 *Mon. Not. R. Astron. Soc.* **299** 1059–68
[10] Regge T and Wheeler J A 1957 *Phys. Rev.* **108** 1063
[11] Edelstein and Vishveshwara C V 1970 *Phys. Rev.* D **1** 3514
[12] Zerilli F J 1970 *Phys. Rev.* D **2** 2141
Zerilli F J 1970 *Phys. Rev. Lett.* **24** 737
[13] Moncrief V 1974 *Ann. Phys., NY* **88** 323–42
[14] Chandrasekhar S 1983 *The Mathematical Theory of Black Holes* (Oxford: Clarendon)
[15] Bruni M, Matarrese S, Mollerach S and Sonego S 1997 *Class. Quantum Grav.* **14** 2585–606
[16] Price R H 1972 *Phys. Rev.* D **5** 2439–54
[17] Bardeen J M and Press W H 1973 *J. Math. Phys.* **14** 7
[18] Gleiser R J, Nicasio C O, Price R H and Pullin J 1996 *Class. Quantum Grav.* **13** L117
Gleiser R J, Nicasio C O, Price R H and Pullin J 1996 *Phys. Rev. Lett.* **77** 4483–86

[19] Zerilli F J 1974 *Phys. Rev.* D **9** 860
[20] Thorne K S 1994 *Black Holes and Time Warps: Einstein's Outrageous Legacy* (New York: Norton)
[21] Misner C W 1963 *Ann. Phys.* **24** 102–17
[22] Wald R M 1979 *J. Math. Phys.* **20** 1056
[23] Detweiler S L 1979 *Sources of Gravitational Radiation* ed L Smarr (Cambridge: Cambridge University Press) pp 211–30
[24] Vishveshwara C V 1970 *Phys. Rev.* D **1** 2870
[25] Nollert H-P 1986 *Proc. 4th Marcel Grossmann Meeting on General Relativity* ed R Ruffini (British Vancouver: Science) pp 759–67
[26] Nollert H-P and Schmidt B G 1992 *Phys. Rev.* D **45** 2617–27
[27] Kay B S and Wald R M 1987 *Class. Quantum Grav.* **4** 893
[28] Smirnov V I 1964 *A Course of Higher Mathematics* (Oxford: Pergamon)
[29] Leaver E W 1986 *Phys. Rev.* D **34** 384
[30] Sun Y and Price R H 1988 *Phys. Rev.* D **38** 1040
[31] Sun Y and Price R H 1990 *Phys. Rev.* D **41** 2492
[32] Price R H and Husain V 1992 *Phys. Rev. Lett.* **68** 1973–76
[33] Andersson N 1997 *Phys. Rev.* D **55** 468
[34] Jensen B P and Candelas P 1986 *Phys. Rev.* D **33** 1590
Jensen B P and Candelas P 1987 *Phys. Rev.* D **35** 4041
[35] Ching E S C, Leung P T, Suen W M and Young K 1995 *Phys. Rev. Lett.* **74** 2414–17
Ching E S C, Leung P T, Suen W M and Young K 1995 *Phys. Rev.* D **52** 2118–32
[36] Gundlach C, Price R and Pullin J 1994 *Phys. Rev.* D **49** 883–9
[37] Nollert H-P and Price R H 1999 *J. Math. Phys.* **40** 980–1010
[38] Bachelot A and Motet-Bachelot A 1993 *Proc. 4th Int. Conf. on Hyperbolic Problems* ed A Donato and F Oliveri (Braunschweig: Vieweg)
[39] Beyer H R 1999 *Commun. Math. Phys.* **204** 397–423
[40] Leung P T, Liu S Y and Young K 1994 *Phys. Rev.* A **49** 3057–67
[41] Ching E S C, Leung P T, Suen W M and Young K 1995 *Phys. Rev. Lett.* **74** 4588–91
Ching E S C, Leung P T, Suen W M and Young K 1996 *Phys. Rev.* D **54** 3778–91
[42] Bachelot A and Motet-Bachelot A 1992 *Ann. Inst. H Poincaré* A **59** 3–68
[43] Nollert H-P 1996 *Phys. Rev.* D **53** 4397–402
[44] Kokkotas K D and Schutz B F 1992 *Mon. Not. R. Astron. Soc* **255** 119
[45] Leins M, Nollert H-P and Soffel M 1993 *Phys. Rev.* D **48** 3467–72
[46] Kokkotas K D 1994 *Mon. Not. R. Astron. Soc.* **268** 1015
Kokkotas K D 1995 *Mon. Not. R. Astron. Soc.* **277** 1599
[47] Kokkotas K D and Schutz B F 1986 *Gen. Rel. Grav.* **18** 913–21
[48] Baumgarte T W and Schmidt B G 1993 *Class. Quantum Grav.* **10** 2067–76
[49] Kokkotas K D 1996 *Proc. Les Houches School on Astrophysical Sources of Gravitational Waves* ed J-A Marck and J P Lasota (Berlin: Springer)
[50] Leung P T, Liu Y T, Tam C Y and Young K 1998 *Phys. Lett.* A **247** 253–60
[51] Beyer H R 1995 *J. Math. Phys.* **36** 4792–814
Beyer H R 1995 *J. Math. Phys.* **36** 4815–25
[52] Beyer H R and Schmidt B G 1995 *Astron. Astrophys.* **296** 722–6
[53] Cunningham C T, Price R H and Moncrief V 1978 *Astrophys. J.* **224** 643
Cunningham C T, Price R H and Moncrief V 1979 *Astrophys. J.* **230** 870–92
[54] Gundlach C, Price R and Pullin J 1994 *Phys. Rev.* D **49** 890–9
[55] Misner C W, Thorne K S and Wheeler J A 1973 *Gravitation* (New York: Freeman)
[56] Weinberg S 1972 *Gravitation and Cosmology: Principles and Applications of the General Theory of Relativity* (New York: Wiley)
[57] Shapiro S L and Teukolsky S A 1983 *Black Holes, White Dwarfs and Neutron Stars: the Physics of Compact Objects* (New York: Wiley)
[58] York J W Jr 1979 *Sources of Gravitational Radiation* ed L L Smarr (London: Cambridge University Press) pp 83–126
[59] Allen G, Andersson N, Kokkotas K and Schutz B F 1998 *Phys. Rev.* D **58** 124012
[60] Ipser J R and Price R H 1991 *Phys. Rev.* D **43** 1768
[61] Kojima Y 1992 *Phys. Rev.* D **46** 4289–303
Kojima Y 1993 *Astrophys. J.* **414** 247–53
[62] Moncrief V 1974 *Ann. Phys., NY* **88** 343

[63] Chandrasekhar S and Ferrari V 1991 *Proc. R. Soc.* A **432** 247–79
[64] Chandrasekhar S and Ferrari V 1991 *Proc. R. Soc.* A **434** 449–57
[65] Kind S, Ehlers J and Schmidt B G 1993 *Class. Quantum Grav.* **10** 2137
[66] Chandrasekhar S 1964 *Astrophys. J.* **140** 417
[67] Detweiler S L and Ipser J 1973 *Astrophys. J.* **185** 685
[68] Lindblom L 1997 *Proc. 14th Int. Conf. on General Relativity and Gravitation* ed M Francaviglia *et al* (Singapore: World Scientific) pp 237–58
[69] Stergioulas N 1998 Rotating stars in relativity *Living Rev. Rel.* pp 1998–8
[70] Chandrasekhar S 1975 *Proc. R. Soc.* A **343** 289
[71] Chandrasekhar S 1980 *Proc. R. Soc.* A **369** 425–33
[72] Price R H and Anderson A 1991 *Phys. Rev.* D **43** 3147
[73] Davis M, Ruffini R, Press W H and Price R H 1971 *Phys. Rev. Lett.* **27** 1466–69
[74] Chandrasekhar S and Detweiler S 1975 *Proc. R. Soc.* A **344** 441
[75] Fröman N, Fröman P O, Andersson N and Hökback A 1992 *Phys. Rev.* D **45** 2609–16
[76] Andersson N 1992 *Proc. R. Soc.* A **439** 47–58
[77] Mashhoon B 1983 *Proc. 3rd Marcel Grossmann Meeting on Recent Developments of General Relativity* ed H Ning (Princeton: Science) pp 599–608
[78] Ferrari V and Mashhoon B 1984 *Phys. Rev. Lett.* **52** 1361
Ferrari V and Mashhoon B 1984 *Phys. Rev.* D **30** 295
[79] Blome H-J and Mashhoon B 1983 *Phys. Lett.* A **100** 231
[80] Schutz B F and Will C M 1985 *Astrophys. J.* **291** L33–6
[81] Iyer S and Will C M 1987 *Phys. Rev.* D **35** 3621
[82] Iyer S 1987 *Phys. Rev.* D **35** 3632
[83] Guinn J W, Will C M, Kojima Y and Schutz B F 1990 *Class. Quantum Grav.* **7** L47
[84] Leaver E W 1985 *Proc. R. Soc.* A **402** 285
Leaver E W 1984 *PhD Thesis* University of Utah, Salt Lake City
[85] Andersson N and Linnæus S 1992 *Phys. Rev.* D **46** 4179
[86] Nollert H-P 1993 *Phys. Rev.* D **47** 5253–58
[87] Andersson N 1993 *Class. Quantum Grav.* **10** L61–L67
[88] Liu H Y 1995 *Class. Quantum Grav.* **12** 543–52
[89] Hod S 1998 *Phys. Rev. Lett.* **81** 4293–96
[90] Andersson N 1995 *Phys. Rev.* D **51** 353
[91] Liu H Y and Mashhoon B 1996 *Class. Quantum Grav.* **13** 233–51
[92] Gal'tsov D B and Matiukhin A A 1992 *Class. Quantum Grav.* **9** 2039–55
[93] Andersson N, Araújo M E and Schutz B F 1993 *Class. Quantum Grav.* **10** 735
[94] Araújo M E, Nicholson D and Schutz B F 1993 *Class. Quantum Grav.* **10** 1127
[95] Andersson N, Araújo M E and Schutz B F 1993 *Class. Quantum Grav.* **10** 757
[96] Chandrasekhar S 1984 *Proc. R. Soc.* A **392** 1
[97] Andersson N 1994 *Class. Quantum Grav.* **11** L39–44
[98] Leung P T, Liu Y T, Suen W-M, Tam C Y and Young K 1997 *Phys. Rev. Lett.* **78** 2894–97
[99] Thorne K S and Campolattaro A 1967 *Astrophys. J.* **149** 591–611
Thorne K S and Campolattaro A 1967 *Astrophys. J.* **152** 673
[100] Detweiler S L and Lindblom L 1985 *Astrophys. J.* **292** 12–15
[101] Lindblom L and Detweiler S L 1983 *Astrophys. J. Suppl.* **53** 73–92
[102] Chandrasekhar S and Ferrari V 1995 *Proc. R. Soc.* A **450** 463–75
[103] Andersson N, Kokkotas K D and Schutz B F 1995 *Mon. Not. R. Astron. Soc* **274** 1039–48
[104] Andersson N, Kojima Y and Kokkotas K D 1996 *Astrophys. J.* **462** 855–64
[105] Thorne K S 1969 *Astrophys. J.* **158** 997
[106] Andersson N, Kokkotas K D and Schutz B F 1996 *Mon. Not. R. Astron. Soc.* **280** 1230
[107] McDermott P N, Horn H M V and Scholl J F 1983 *Astrophys. J.* **268** 837
McDermott P N, Horn H M V and Hansen C J 1988 *Astrophys. J.* **325** 725
[108] Schutz B F 1991 *Phys. World* **4** 24
[109] Andersson N 1996 *Gen. Rel. Grav.* **28** 1433–45
[110] Andersson N and Kokkotas K D 1998 *Mon. Not. R. Astron. Soc.* **297** 493–6
[111] Abramowicz M A, Andersson N, Bruni M, Ghosh P and Sonego S 1997 *Class. Quantum Grav.* **14** L189–94
[112] Nollert H-P 1998 *Proc. 8th Marcel Grossmann Meeting on General Relativity* (Singapore: World Scientific)
[113] Abrahams A M and Price R H 1996 *Phys. Rev.* D **53** 1963–71
[114] Nollert H-P 1999 *Proc. 19th Texas Symp.*

[115] Oohara K-i and Nakamura T 1984 *Prog. Theor. Phys.* **71** 91–9
Oohara K-i 1984 *Prog. Theor. Phys.* **71** 738
[116] Lousto C O and Price R H 1997 *Phys. Rev.* D **55** 2124–38
[117] Allen G, Camarda K and Seidel E 1998 *Preprint* gr-qc/9806036 (*Phys. Rev. Lett.* submitted)
[118] Andersson N and Kokkotas K D 1996 *Phys. Rev. Lett.* **77** 4134
[119] Creighton J D E 1997 *7th Canadian Conf. on General Relativity and Relativistic Astrophysics*
[120] Kokkotas K D, Apostolatos T A and Andersson N 1999 *Preprint* gr-qc/9901072 (*Mon. Not. R. Astron. Soc.* to be published)
[121] Merkowitz S M and Johnson W W 1997 *Phys. Rev.* D **56** 7513–28
[122] Flanagan E E 1998 *Proc. 15th Int. Conf. on General Relativity and Gravitation* ed N Dadhich and J Narlikar (Pune: Inter-University Centre for Astronomy and Astrophysics) pp 177–97
[123] Danzmann K 1998 *Relativistic Astrophysics* ed H Riffert *et al* (Braunschweig: Vieweg) pp 48–65
[124] Finn L S 1997 *Proc. 2nd Eduardo Amaldi Meeting*
[125] Schutz B F 1997 Proc. 1997 *Alpbach Summer School on Fundamental Physics in Space* ed A wilson (Noordwijk: ESA) pp 265–84
[126] Helstrom C W 1968 *Statistical Theory of Signal Detection* (Oxford: Pergamon)
[127] Tominaga K, Saijo M and Maeda K-i 1999 *Phys. Rev.* D **60** 024004
[128] Ferrari V, Gualtieri L and Borrelli A 1999 *Phys. Rev.* D **59** 124020
[129] Andrade Z and Price R H 1999 *Phys. Rev.* D **60** 104037
[130] Ruoff J and Laguna P 1999 *Phys. Rev.* D submitted
[131] Allen G, Andersson N, Kokkotas K, Laguna P, Pullin J and Ruoff J 1999 *Phys. Rev.* D **60** 104021
(Allen G, Andersson N, Kokkotas K, Laguna P, Pullin J and Ruoff J 1999 *Preprint* gr-qc/9903100)
[132] York J W Jr 1989 *Frontiers in Numerical Relativity* ed C R Evans *et al* (Cambridge: Cambridge University Press) pp 89–109
[133] Walter F M and Matthews L D 1997 *Nature* **389** 358–60
[134] Thorne K S 1998 *Black Holes and Relativistic Stars* ed R M Wald (Chicago, IL: University of Chicago Press)
[135] Flanagan E E and Hughes S A 1998 *Phys. Rev.* D **57** 4535–65
Flanagan E E and Hughes S A 1998 *Phys. Rev.* D **57** 4566–87
[136] Nicholson D and Vecchio A 1998 *Phys. Rev.* D **57** 4588–99
[137] Brady P R, Creighton T, Cutler C and Schutz B F 1998 *Phys. Rev.* D **57** 2101–16
[138] Kojima Y 1987 *Prog. Theor. Phys.* **77** 297–309
[139] Kokkotas K D and Schmidt B G 1999 *Living Rev. Rel.* **2** 1999-2
[140] Teukolsky S A 1972 *Phys. Rev. Lett.* **29** 1114
Teukolsky S A 1973 *Astrophys. J.* **185** 635
[141] Krivan W, Laguna P and Papadopoulos P 1996 *Phys. Rev.* D **54** 4728
Krivan W, Laguna P and Papadopoulos P 1997 *Phys. Rev.* D **56** 3395–404
[142] Detweiler S 1980 *Astrophys. J.* **239** 292
[143] Seidel E and Iyer S 1990 *Phys. Rev.* D **41** 374
[144] Kokkotas K D 1991 *Class. Quantum Grav.* **8** 2217
[145] Onozawa H 1997 *Phys. Rev.* D **55** 3593–602
[146] Zel'dovich Y B 1972 *Sov. Phys.–JETP* **35** 1085
[147] Andersson N, Laguna P and Papadopoulos P 1998 *Phys. Rev.* D **58** 087503
[148] Hartle J B 1967 *Astrophys. J.* **150** 1005
Hartle J B and Thorne K S 1968 *Astrophys. J.* **153** 807
[149] Butterworth E M and Ipser J R 1976 *Astrophys. J.* **204** 200
[150] Komatsu H, Eriguchi Y and Hachisu I 1989 *Mon. Not. R. Astron. Soc.* **239** 153
[151] Neugebauer G and Herlt E 1984 *Class. Quantum Grav.* **1** 695
[152] Neugebauer G and Herold H 1992 *Relativistic Gravity Research (Lecture Notes in Physics vol 410)* ed J Ehlers and G Schäfer (Berlin: Springer) pp 305–18
[153] Wu X, Müther H, Soffel M, Herold H and Ruder H 1991 *Astron. Astrophys.* **246** 411–6
[154] Herold H 1996 *Relativity and Scientific Computing: Computer Algebra, Numerics, Visualization* ed F W Hehl *et al* (Heidelberg: Springer) pp 122–37
[155] Bonazzola S, Gourgoulhon E and Marck J-A 1998 *Phys. Rev.* D **58** 104020
[156] Stergioulas N and Friedman J L 1995 *Astrophys. J.* **444** 306–11
[157] Lousto C O 1999 *MPI report* AEI-1999–29
[158] Kojima Y 1993 *Prog. Theor. Phys.* **90** 977–90
[159] Cutler C 1991 *Astrophys. J.* **374** 248
Cutler C and Lindblom L 1992 *Astrophys. J.* **385** 630

Lindblom L 1995 *Astrophys. J.* **438** 265
[160] Yoshida S and Kojima Y 1997 *Mon. Not. R. Astron. Soc.* **289** 117
[161] Stergioulas N and Friedman J L 1998 *Astrophys. J.* **492** 301
[162] Chandrasekhar S 1970 *Phys. Rev. Lett.* **24** 611
Friedman J L and Schutz B F 1978 *Astrophys. J.* **222** 281
[163] Andersson N 1998 *Astrophys. J.* **502** 708–13
Friedman J L and Morsink S M 1998 *Astrophys. J.* **502** 714–20
[164] Andersson N, Kokkotas K and Schutz B F 1999 *Astrophys. J.* **510** 846–53
[165] Owen B J, Lindblom L, Cutler C, Schutz B F, Vecchio A and Andersson N 1998 *Phys. Rev.* D **58** 084020